IRIS AperTO

UNIVERSITÀ DEGLI STUDI DI TORINO

AperTO - Archivio Istituzionale Open Access dell'Università di Torino

New aldo-keto reductase 1C3 (AKR1C3) inhibitors based on the hydroxytriazole scaffold

This is a pre print version of the following article:

Original Citation:

Availability:

This version is available http://hdl.handle.net/2318/1859921 since 2022-06-21T14:25:58Z

Published version:

DOI:10.1016/j.ejmech.2022.114366

Terms of use:

Open Access

Anyone can freely access the full text of works made available as "Open Access". Works made available under a Creative Commons license can be used according to the terms and conditions of said license. Use of all other works requires consent of the right holder (author or publisher) if not exempted from copyright protection by the applicable law.

(Article begins on next page)

19 April 2024

New Aldo-Keto Reductase 1C3 (AKR1C3) inhibitors based on the hydroxytriazole scaffold

Agnese Chiara Pippione,[1#] Zühal Kilic-Kurt,[2#] Sandra Kovachka,[1,3] Stefano Sainas,[1] Barbara Rolando,[1] Enrica Denasio,[4] Klaus Pors,[4] Salvatore Adinolfi,[1] Daniele Zonari,[1] Renzo Bagnati,[5] Marco Lucio Lolli,[1] Francesca Spyrakis,[1*] Simonetta Oliaro-Bosso[1*] and Donatella Boschi[1*]

[#]these authors contributed equally to the work

[1] *Department of Science and Drug Technology, University of Turin, via Pietro Giuria 9, 10125 Turin (Italy).*

[2] *Ankara University, Faculty of Pharmacy, Department of Pharmaceutical Chemistry, Ankara, Turkey.*

[3] *current address: Université Côte d'Azur, CNRS, ICN, 28 Avenue Valrose, 06108 Nice, CEDEX 2, France.*

[4] *Institute of Cancer Therapeutics, Faculty of Life Sciences, University of Bradford, West Yorkshire BD7 1DP (U.K).*

[5] *Department of Environmental Health Sciences, Istituto di Ricerche Farmacologiche Mario Negri IRCCS, Via Mario Negri 2, 20156 Milan (Italy).*

Abstract

The aldo-keto reductase 1C3 (AKR1C3) enzyme is considered an attractive target in Castration Resistant Prostate Cancer (CRPC) because of its role in the biosynthesis of androgens. Flufenamic acid, a non-selective AKR1C3 inhibitor, has previously been subjected to bioisosteric modulation to give rise to a series of compounds with the hydroxytriazole core. In this work, the hit compound of the previous series has been modulated further, and new, more potent, and selective derivatives have been obtained. The poor solubility of the most active compound (cpd **5**) has been improved by substituting the triazole core with an isoxazole heteronucleous, with similar enzymatic activity being retained. Potent AKR1C3 inhibition is translated into antiproliferative effects against the 22RV1 CRPC cellular model, and the *in-silico* design, synthesis and biological activity of new compounds is described herein. Compounds have also been assayed in combination with two approved antitumor drugs, abiraterone and enzalutamide.

1. Introduction

17α-hydroxysteroid dehydrogenase type 5 (HSD17B5), also known as aldo-keto reductase type 1C3 (AKR1C3), is a cytosolic enzyme member of the AKR1C 1-4 aldo-keto reductase family.[1] These phase 1 metabolic enzymes are dependent on nicotinamide adenine dinucleotide phosphate (NADPH) and play their crucial roles in the reduction of ketosteroids. Although AKR1C 1-4 isoforms share high sequence homology (> 86%), they have different biological functions and distribution preferences. In particular, C3 is mostly expressed in the endocrine organs, such as the adrenal glands, breast, uterus and prostate, where it is involved in the *de-novo* biosynthesis of steroids by reducing the 17-ketosteroid function and converting Δ^4-androstene-3,17-dione and 5α-androstane-3,17-dione to testosterone and 5α-dihydrotestosterone (DHT), respectively. Both testosterone and DHT are potent androgens with a high affinity for the androgen receptor (AR). Notably, in the prostate, C2 and C3 have completely contrasting catalytic functions in DHT activation; the inhibition of C3 can be effective in the treatment of prostate cancer (PC),[2] while inhibiting the C2 isoform can promote proliferative signaling. Accordingly, selective C3 over C2 inhibition is essential in treating CRPC as it can circumvent undesirable 1C isoform-related side effects. AKR1C3 has also been shown to play a role in resistance to pharmacological and radiation therapy[2-4]. Two drugs currently used for the clinical treatment of CRPC, enzalutamide (ENZA) and abiraterone (ABI), are associated with drug resistance that emerges within few months.[5, 6] Specifically, AKR1C3 overexpression contributes to ABI and ENZA resistance by providing a source of intratumoral androgens, which can be surmounted to some extent either via the administration of indomethacin (INDO), a known AKR1C3 inhibitor that also inhibits COX isozymes,[7, 8] or more selective AKR1C3 inhibitors.[9] Through its role as a carbonyl reductase, C3 also mediates the inactivation and resistance of doxorubicin and other anthracyclines,[10, 11] while it has been confirmed as a radioresistance-associated gene for PC,[4] esophageal cancer,[12, 13] and non-small cell lung cancer (NSCLC).[14] Malignant cells can become radioresistant by upregulating C3 expression to decrease cell apoptosis, eliminating reactive oxygen species (ROS), accumulating prostaglandin PGF2α for the further activation of the MAPK signaling pathway and inhibiting G2/M phase arrest.[4, 12-14] To date, no selective AKR1C3 inhibitor has been successfully approved for clinical use. The clinical studies of ASP9521 (NTC01352208 for CRPC, Figure 1) and BAY-1128688 (NCT03373422 for endometriosis) were terminated; ASP9521 lacked measurable clinical therapeutic activity,[15] whereas BAY-1128688 was terminated early due to hepatotoxicity (on ClinicalTrials.gov). An ongoing trial is focusing on evaluating the efficacy of the non-selective AKR1C3 inhibitor INDO in combination with ENZA for the treatment of CRPC (NCT02935205). Given the complexity of the steroidogenic pathway and escape mechanisms following response to treatment with ABI and ENZA, AKR1C3 is an attractive target for therapeutic intervention. In a very comprehensive review[2], Liu *et al*. reported the most representative AKR1C3 inhibitors discovered until now. Some of them were developed from natural compounds, like berberine [16] or baccharin (Figure 1);[10] others were developed from off-label use compounds, like the cyclin-dependent kinase inhibitors roscovitine and purvalanol A, the antidiabetic agents sulfonylureas glimepiride and gliclazide,[17] non-steroidal anti-inflammatory drugs (NSAID) analogues like naproxene,[18] INDO[19] and flufenamic acid (FLU)[20-22]. The properties of new AKR1C3 inhibitors developed from known drugs required improved C3 target selectivity and reduced off-target effects to minimize systemic toxicity. The aforementioned NSAID derivatives contain a carboxyl acid group, which is known to render their entry into cells dependent on specific monocarboxylic acid transporters.[23] As differences in cell permeability are often responsible for inconsistencies in *in vitro* and *in vivo* activity experiments, the development of non-carboxylic acid inhibitors could limit or completely avoid thetransporter-mediated processes. To address this, High-Throughput Screening were employed to identify the potent carboxylic acid-free based compounds morpholinurea derivative SN34037 and the phenylpyrrolidin-2-one SN33638 (Figure 1). In order to circumvent the transporter-mediated processes and improving bioavailability, we recently[24, 25], applied bioisosteric and scaffold-hopping techniques to the structure of two NSAIDs, INDO,[26] and FLU,[25] designing for the discovery of more potent and more selective AKR1C3 inhibitors.

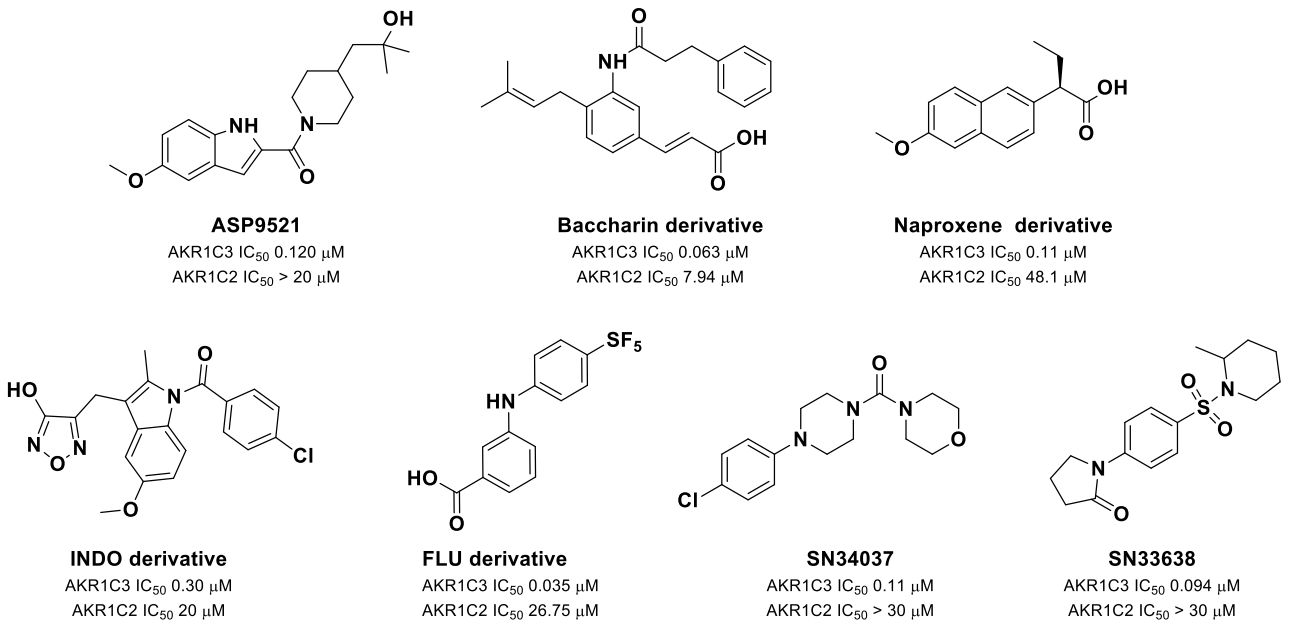

Figure 1: Structures of most representative AKR1C3 inhibitors developed so far. For each lead (ASP9521,[27] baccharin derivative,[28] naproxene derivative,[18] INDO[26] and FLU[20] derivatives, SN34037[29] and SN33638[30]) the IC_{50} values on AKR1C3 and C2 isoforms are reported.

Specifically, we have previously replaced the benzoic acid moiety of FLU with an acidic hydroxyazolecarbonylic scaffold in order to diminish its off-target effects on AKR1C2 and cyclooxygenase (COX1 and 2).[31] Several N-substituted hydroxylated triazoles were designed to simultaneously interact with both sub-pockets 1 and 2, as they are larger in AKR1C3 than in other AKR1C isoform active sites.[17] Through X-ray structural studies, computational design and iterative rounds of synthesis and biological evaluation, novel compounds were reported and these shared high selectivity (up to 460-fold) for C3, over the C2 isoform, and minimal COX1 and COX2 off-target inhibition (compound **1**, Figure 2).[31] A further conformational restriction approach was then employed to improve the potency and selectivity of FLU, resulting in the design of a focused library of 3-hydroxybenzoisoxazole-based compounds, in which the carboxylic acid substituent of FLU was fused with the benzene ring in order to constrain one of the FLU conformations (compound **2**, Figure 2). The structure determination of AKR1C3 co-crystallized with **1** and **2**,[31] the two most potent compounds of the two series, clearly identified both compounds in the androstenedione binding site. Importantly, the design supported biochemical data, demonstrating the ability of both bioisosteric approaches to effectively mimic the carboxylic group of FLU in the oxyanion site (OS) of the AKR1C3 enzyme. Moreover, the two co-crystallized compounds were revealed to have the same binding contacts within the SP1 and SP2 pockets as the reference FLU. Compound **1** displayed a promising interaction in sub-pocket 3 via the 4-methoxybenzyl moiety and, as this was different to FLU, it served as a key point in the design of new, more potent and selective AKR1C3 inhibitors from scaffold **A** (Figure 1). The bis-trifluoromethylphenyl substituent of compound **2** projects deeply into the SP1 pocket, with this pocket being larger in the C3 isoform than in C2 according to the crystallographic data on AKR1C isoforms. These observations, combined with the molecular-docking studies, have guided the design of the new hydroxytriazole series. In fact, in this work, we describe a structure-guided lead-optimization program around the 4-hydroxy-1-*p*-methoxybenzylazole scaffold leading to the identification of potent and selective AKR1C3 inhibitors. In addition to the design and synthetic strategies employed, we also present biochemical and cell-

based studies on the new compounds, used alone and in combination with ABI and ENZA. Finally, we demonstrate that their AKR1C3 inhibition impacts upon both testosterone- and PSA-synthesis levels.

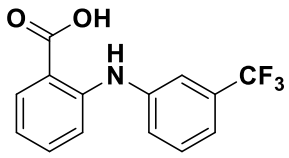

Flufenamic acid
IC_{50} on AKR1C3: 0.44 μM
IC_{50} on AKR1C2: 0.53 μM
IC_{50} on COX1: 14 μM

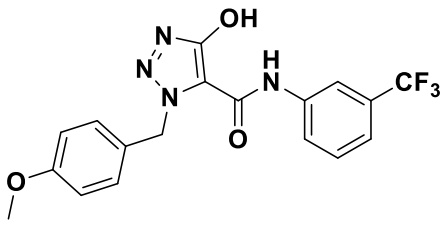

1
IC_{50} on AKR1C3: 0.31 μM
IC_{50} on AKR1C2: 73.23 μM
IC_{50} on COX1: >100 μM

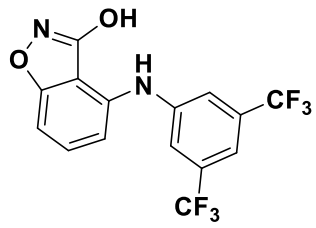

2
IC_{50} on AKR1C3: 0.26 μM
IC_{50} on AKR1C2: 118.55 μM
IC_{50} on COX1: >100 μM

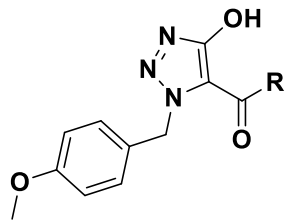

Scaffold A

Figure 2. Flufenamic acid, an unselective inhibitor of AKR1C3, and bioisostere C3 *vs* C2 selective derivatives **1** and **2**.[25, 31] Scaffold A, the common structure of the compounds here described, is also shown.

2. Results and discussion

2.1 In silico guided design of new hydroxyazole-based inhibitors

In the following section, we report the design of a new series of hydroxytriazole-based inhibitors, starting from the previously published compound **1** (Figures 3 and 4).[25]
As reported, hydroxyazole derivatives are known to be deprotonated at physiological pH and are, indeed, good isosteres of the carboxylic function.[32, 33] All simulations, therefore, only considered the deprotonated state of the compounds. The design was performed starting from previous analyses,[25] and from the crystallographic structure of AKR1C3 complexed with compound **1** (PDB ID 6f2u,[31] Figure 3a), which led to the identification of crucial residues for complex stabilization and of the five characteristic compartments (an oxyanion site (OS), a steroid channel and sub-pockets SP1, SP2 and SP3) of the enzyme active site.[24, 34] Compound **1** properly fits in the oxyanion site (NADP+, Try55, His117) via direct H-bonding to Tyr55, His117 and NADP+ (Figure 3a). SP1 (Ser118, Met120, Asn167, Tyr216, Phe306, Phe311, Pro318 and Tyr319) is occupied by the trifluoromethyl group of the trifluoromethyl-phenyl moiety, while the same phenyl group interacts with SP2 (Trp86, Leu122, Ser129, Phe311). This latter also hosts the methoxybenzyl moiety, which mainly occupies SP3 (NADP+, Tyr24, Glu192, Ser217, Ser221, Gln222, Asp224, Trp227, Tyr305). A more careful inspection of the binding site led to the identification of empty regions in SP1, which

are delimited by residues Phe306 and Tyr319, and in SP2, by Trp86 and Leu122. We thus designed a series of new derivatives with the aim of occupying the empty space and increase compound affinity and activity. The applied docking procedure (see Materials and Methods for further details) was verified by redocking the co-crystallized compound **1**. As shown in Figure 3b, the docked pose is quite similar to the crystallographic one, with the only exception being the methoxybenzyl moiety, which assumes a slightly rotated orientation (Figure 3b). Interestingly, the methoxy group corresponds to an area of poor electron density, making it reasonable to assume that the group, which is not stabilized by any direct or water-mediated contact, may present a certain level of flexibility.

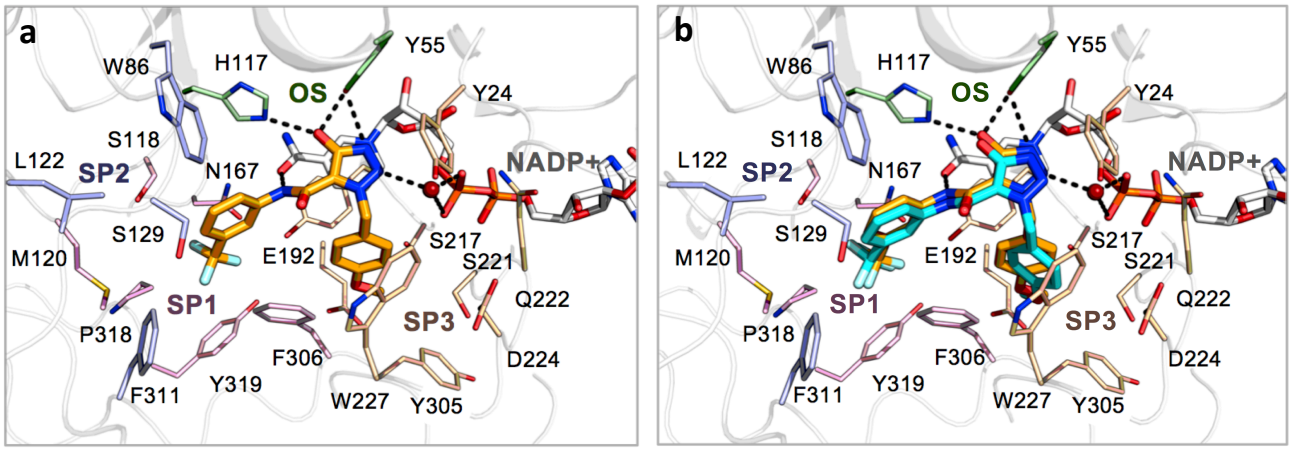

Figure 3. a. X-ray pose of compound **1** in AKR1C3 binding site (PDB ID 6f2u). **b.** Comparison of the X-ray pose with the docked pose of compound **1**. The ligand and residues lining the pocket are shown as sticks. Residues are labeled and colored differently according to the compartment they belong to. The protein is shown as a white transparent cartoon.

All newly designed compounds, which are depicted in Figure 4, present groups that are bulkier than the trifluoromethyl-phenyl moiety and are likely to better occupy the SP1 and SP2 subsites. The addition of another trifluoromethyl group, as in compound **3**, slightly extended contact with SP1, and partially SP2, allowing a closer hydrophobic interaction with Tyr319 to form. In compounds **4** and **5**, the substituent was replaced by a biphenyl that was attached to the amide in the para and meta positions, respectively, to investigate which position would better fit the binding site.

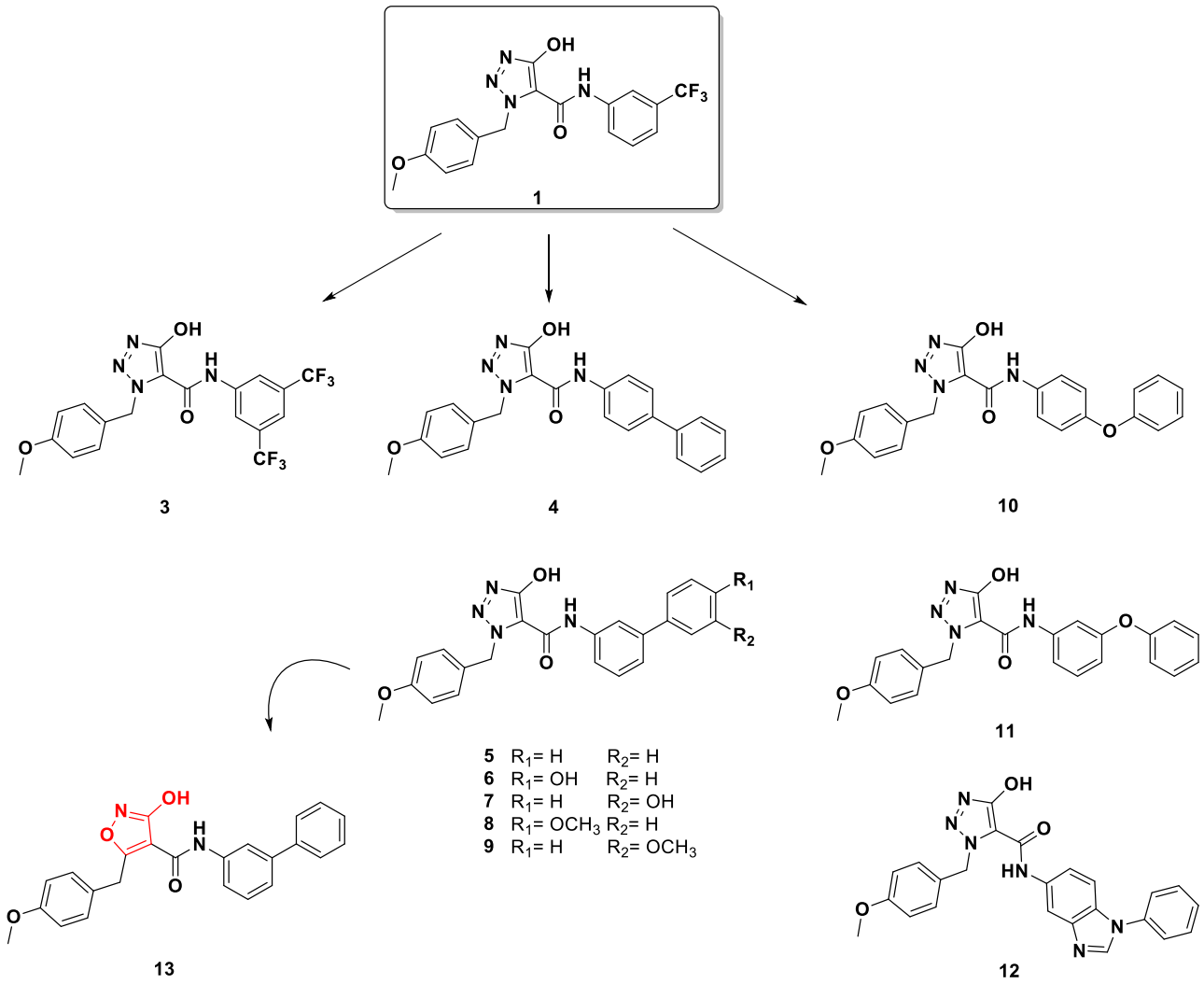

Figure 4. Chemical structures of the hydroxyazole-based AKR1C3 inhibitors studied in this work.

The docking simulations indicated that compound **5** has a more favorable and adaptable pose in the binding pocket. Specifically, two equally reasonable poses, one that better filled SP1 and the other SP2, were produced (Figure 5a). The pose directed towards SP1 (purple ligand) forms additional hydrophobic contacts with Phe308, Pro318 and Tyr319, while the pose oriented towards SP2 (pink ligand) contacts Trp86 and Phe311.

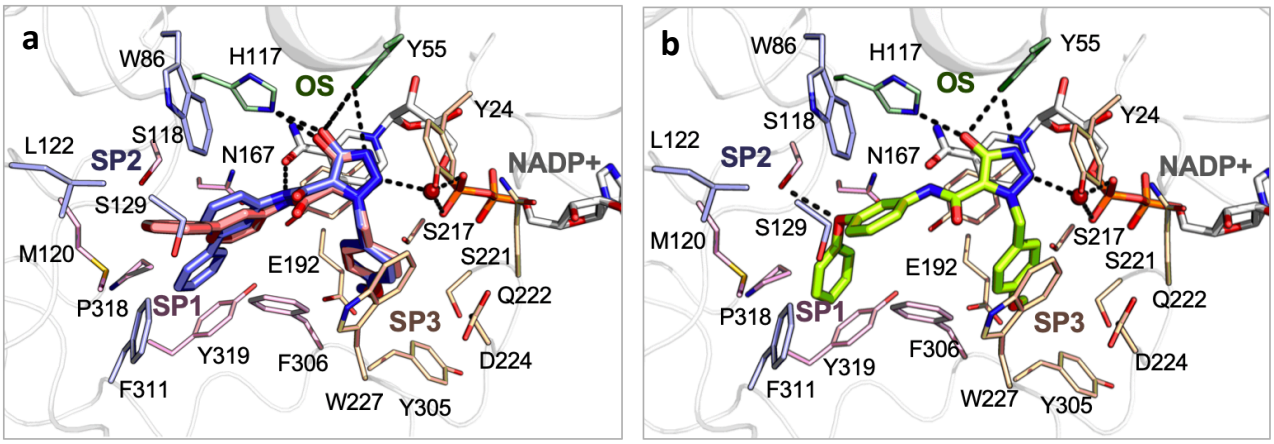

Figure 5. Docking poses of compounds **5** (**a**) and **11** (**b**) in AKR1C3 binding site. The ligands and residues lining the pocket are shown as sticks. Residues are labeled and colored differently according to the sub-pockets they belong to. The protein is shown as a white transparent cartoon. In **a**, compound **5** is shown in two different and equally probable poses, according to docking simulations.

To better understand which binding mode produced the most stable complex, we thus submitted the two docking poses of the compound, in complex with AKR1C3, to a 200 ns-long molecular dynamics (MD) (Figure 6). Both poses were found to be quite stable in the MD simulations, and both maintained the principal H-bonds originally established upon docking. The substituents, however, experienced higher mobility in the first pose (Figure 6a), while the second orientation experienced a more stable and conserved binding (Figure 6b). Moreover, the protein underwent less adjustment and only the water present in the original crystallographic structure was maintained. We thus assumed this last orientation to be the most probable and stable, as also confirmed by the poses obtained for the other compounds in the series (see following paragraph).

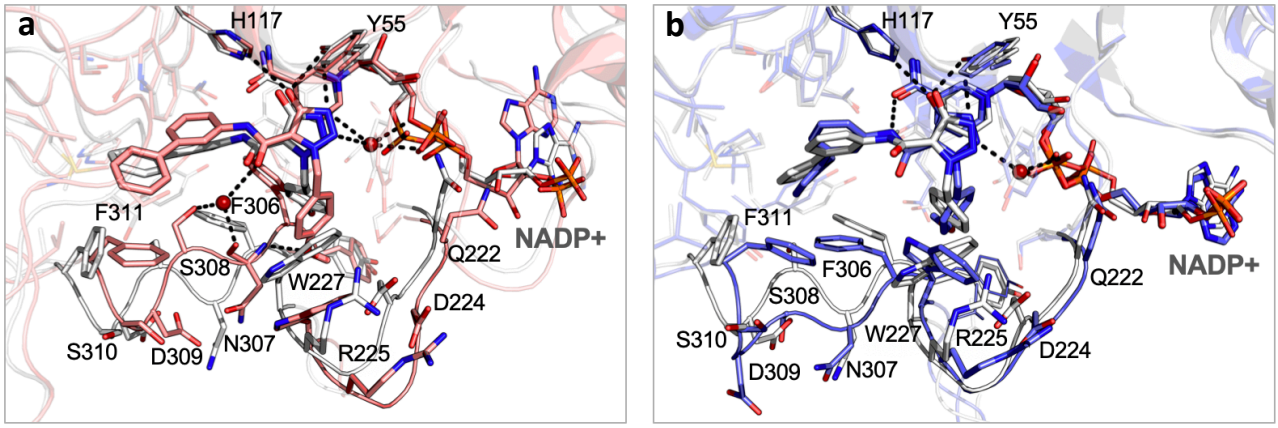

Figure 6. Comparison of the two docking poses (**a** and **b,** grey colored) of compound **5** with the conformations obtained after 200 ns MD (**a** and **b**, pink and purple colored, respectively). The ligands and residues lining the pocket are shown as sticks. AKR1C3 is shown as a transparent cartoon.

In an attempt to increase polar interactions, we then searched for polar residues in SP1 and SP2 that could be contacted by modified substituents. We identified Ser118, Tyr 216 and Tyr319 and Met120 backbone as possible H-bond acceptor groups. Compound **5** was therefore hydroxylated at the para and meta positions of the second benzene ring, generating compounds **6** and **7**, respectively. When docked in the enzyme-binding pocket, compound **6** was able to contact Met120 backbone, but at a distance of 3.4 Å. Compound **7** extended binding to Tyr216 at a better distance (1.8 Å), but also showed multiple different orientations in its docking poses, thus suggesting a lack of stability. The corresponding methoxylated synthetic precursors, compounds **8** and **9**, were also docked in the binding site without leading to any apparent improvement but showed variability in the generated poses.

Subsequently, we investigated the possibility of reaching Ser118 by substituting the biphenyl with a meta or para phenoxyphenyl group, and obtained compounds **10** and **11**, respectively. The docking of **10** and **11** returned quite similar poses and scores. However, although the distance between Ser118 side-chain and the ethereal oxygen (about 3 Å; Figure 5b) allowed a polar contact to be formed, the geometrical orientation was not very favorable.

Following these observations, we designed compound **12** to check whether an even bulkier substituent could better occupy the SP1 and SP2 cavities. The docking of **12** returned two different

poses that displayed several clashes with the residues lining the cavity, suggesting that such a bulky ligand cannot be easily accommodated. Finally, considering that the best binding fit was shown by compound **5**, we decided to maintain the same decorations, but substitute the hydroxyazole scaffold with an isoxazole (compound **13**). The docking results revealed that **13** maintained the same orientation as one of the poses obtained for compound **5** (purple ligand in Figure 5a), apart from the rotation of the amidic group, which led to the loss of the H-bond with the NADP+ amidic terminal and Tyr55, and a slight adjustment of methoxybenzyl moiety. The lipophilic substituent formed hydrophobic interactions with Trp86 (SP2), Met120, Phe306, Pro318 and Tyr319 (SP1).

2.2 Chemistry

a. Synthesis

The methodology used for the synthesis of the hydroxytriazole derivatives **3-12** is described in Scheme 1. The protected triazole building block **14**, which has already been described in our group's preceding papers,[35-37] was converted into the corresponding acyl chloride and allowed to react with the appropriate aniline. While the anilines for the preparation of derivatives **15a-15f** and **16a** were commercially available, the corresponding aniline for **16b** was prepared as previously described.[38, 39] Aniline **19**, used for the synthesis of **15g**, was prepared according to Scheme 2 via a Suzuki cross-coupling reaction. The benzyl protective group was removed from **15a** and **16a** via catalytic hydrogenation, while compounds **15b-g** and **16b** were converted to the final compounds via treatment with trifluoroacetic acid (TFA) in the presence of thioanisole, which was used as a scavenger of the benzylic cation. This second procedure was applied when the low solubility of the final compounds prevented their separation from the catalyst.

As the purification of **15c** (the synthetic precursor of **6**) was not optimal, because of its increased lipophilicity, we decided to prepare **7** using a procedure that is different to that of its analogue **6**. This new procedure entailed a Suzuki reaction to convert **15h** to generate target compound **7** (see Scheme 1).

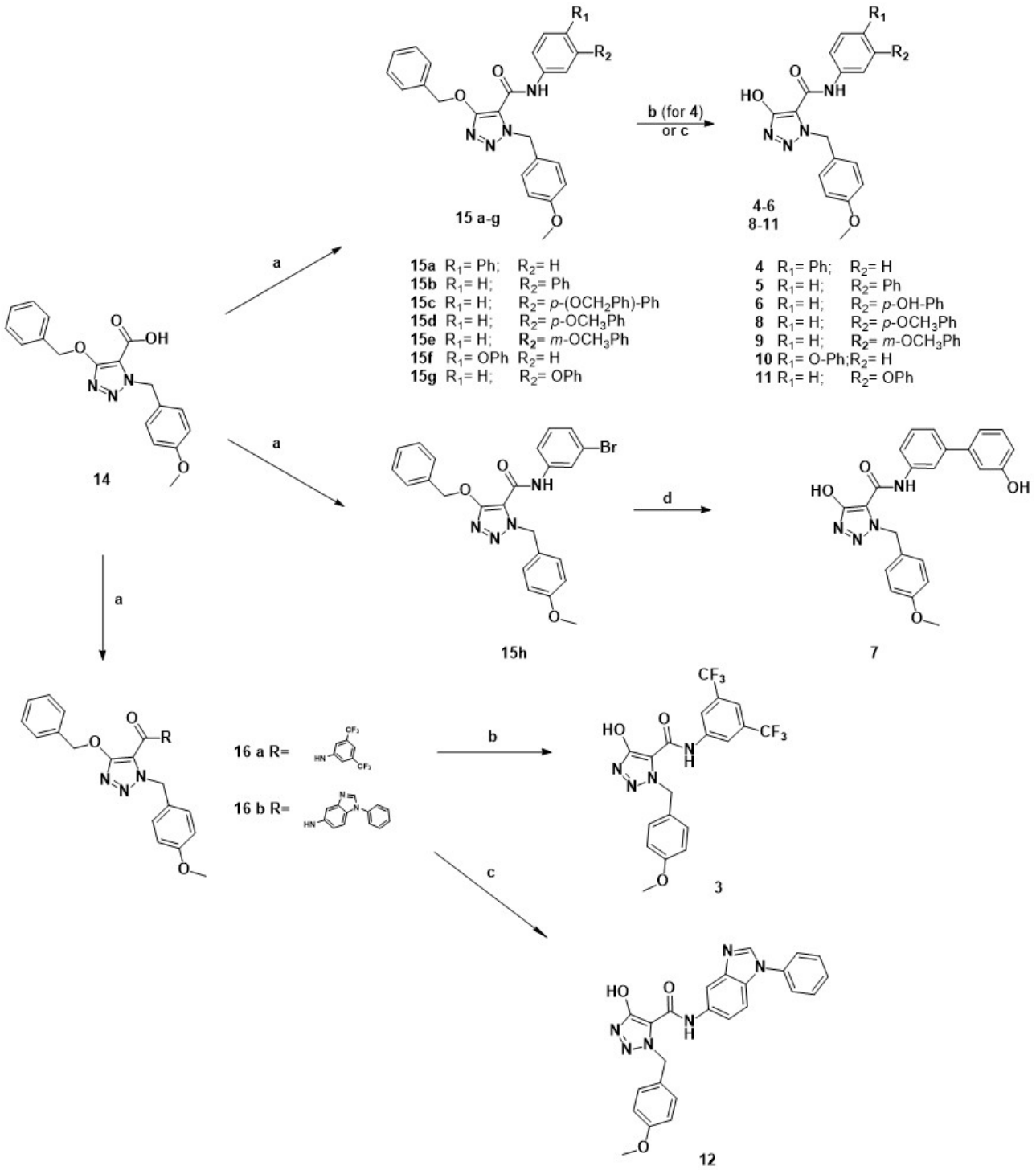

Scheme 1. Synthesis of target hydroxytriazole derivatives **3**-**12**. Reagents and conditions: a) 1) $(CO)_2Cl_2$, dry DMF, dry THF, rt; 2) appropriate aniline, dry pyridine, dry toluene, 70 °C; b) H_2, Pd/C, THF, rt; c) TFA, thioanisole, rt; d) $Pd[(C_6H_5)_3P]_4$, K_2CO_3, dioxane/water (8:2 v/v), (3-hydroxyphenyl)boronic acid, reflux.

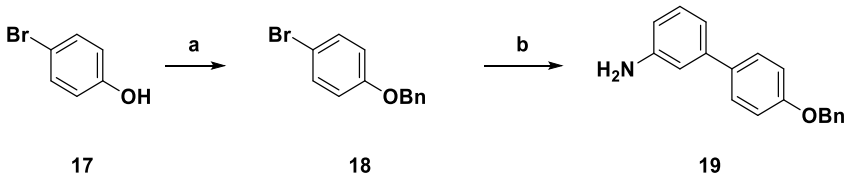

Scheme 2. Synthesis of 4'-(benzyloxy)-[1,1'-biphenyl]-3-amine **19**. Reagents and conditions: a) benzyl bromide, K_2CO_3, dry acetonitrile; b) $Pd[(C_6H_5)_3P]_4$, K_2CO_3, dioxane/water (8:2 v/v), (3-aminophenyl)boronic acid, reflux.

The synthesis of hydroxyisoxazole **13** was performed in accordance with Scheme 3. First, hydroxyisoxazole **22** was synthesized using the method, proposed by Nicolaou *et al.,*[40] for producing a 5-methyl-3-hydroxyisoxazole analogue. Briefly, 2-(4-methoxyphenyl)acetic acid was converted into the corresponding acyl chloride and used for the acylation of dimethyl malonate. The resulting compound **20** was methylated with Me_2SO_4 to selectively grant product **21**. Notably, the use of a different methylating agent (CH_3I) gave rise to a mixture of alkylated products. Ring closure was obtained by treating malonate **21** with NH_2OH in methanol, and subsequently precipitating pure compound **22** from the reaction mixture after acidification to pH 1. The hydroxy group of **22** was selectively protected with a benzyl group using Ag_2O in a benzylation reaction, as described by Nicolaou *et al.*[40] for similar hydroxyisoxazoles. The subsequent hydrolysis of **23** and the coupling of the chloride of the resulting acid **24** with 3-aminobiphenyl gave compound **25**, which was finally deprotected, via hydrogenation at atmospheric pressure, to give **13**.

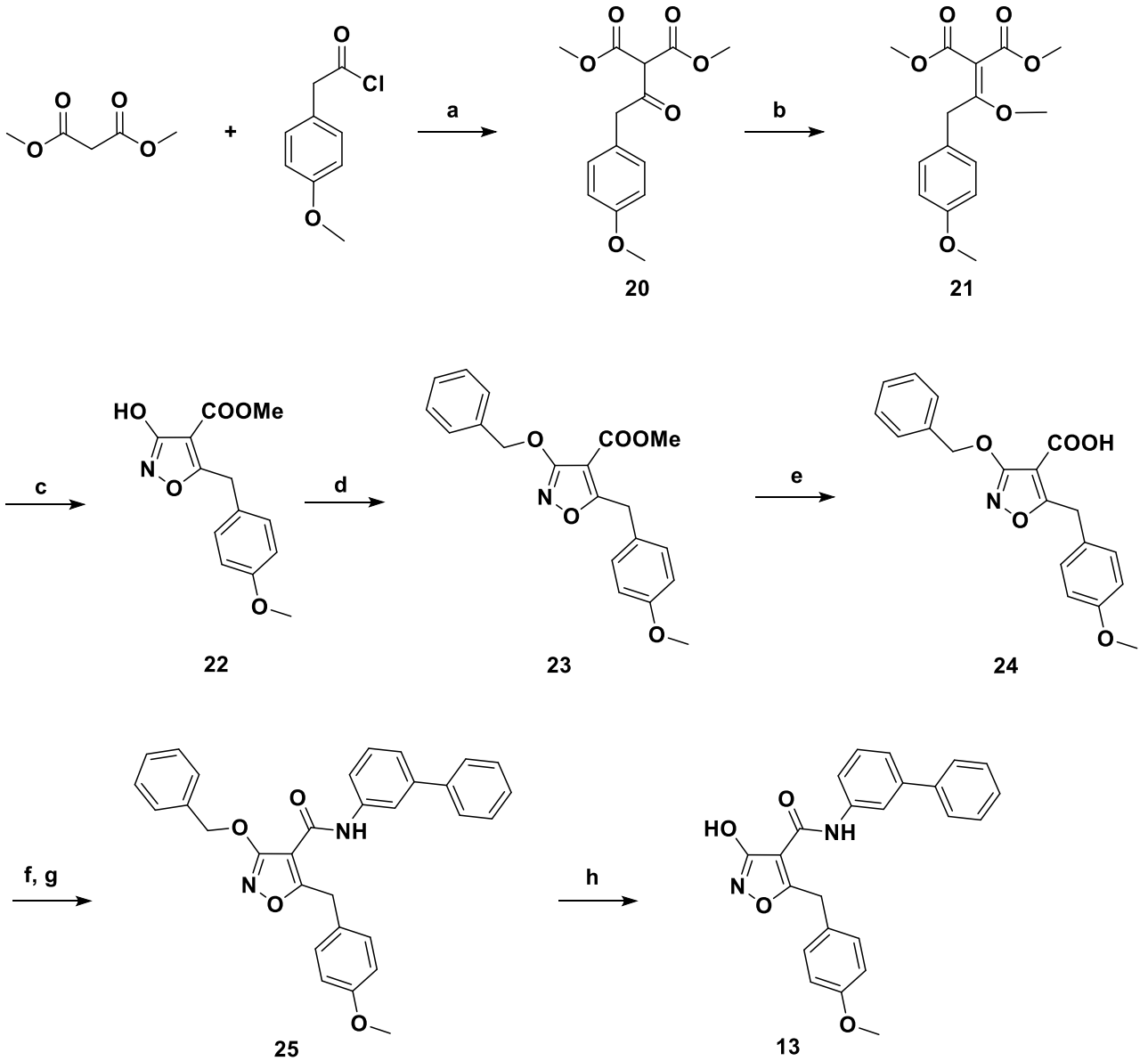

Scheme 3. Synthesis of hydroisoxazole derivative **13**. Reagent and conditions: a) $MgCl_2$, pyridine, DCM, rt; b) Me_2SO_4, DMF, K_2CO_3, rt; c) Na, $NH_2OH \cdot HCl$, MeOH, rt; 2 N aq. HCl d) BnBr, Ag_2O, DMF, rt; e) NaOH, MeOH, 50°C, reflux; f) $(CO)_2Cl_2$, DMF, dry THF, rt; g) 3-aminobiphenyl, pyridine, dry THF, rt; h) H_2, Pd/C, THF.

b. Physicochemical characterization: drug-like properties (pKa, logD, solubility)

The determination of the main physicochemical parameters of the compounds, which define their drug-like properties, was carried out. Solubility at physiological pH was evaluated in phosphate buffered saline (PBS, pH 7.4) at 25 °C, and the results are reported in Table 2. All the triazole derivatives **3-12** showed lower solubility than **1**, except for compound **7**, which showed a solubility twice that of **1** because of its polar ionizable phenolic function. Notably, the higher solubility of isoxazole derivative **13,** compared to triazole analogue **5**, shows the favorable contribution of the isoxazole ring. The isoxazole ring also has an influence on the acidity of the hydroxylic function, as evidenced by the lower pK_a value of **13** than that of the triazole **7**. Specifically, the measured pK_a of the hydroxy function on the triazole ring (compound **7**) was 4.9, while it was 4.5 when the function was positioned on the isoxazole ring (compound **13**). The solubility of compounds **4**, **5** and **8**-**11** was not measurable because the value was lower than the limit of detection (<1 μM) of the UHPLC method used for the quantitative analyses. Lipophilicity was determined at physiological pH ($logD^{7.4}$) using PBS/*n*-octanol as the model system. With the exception of compounds **10** and **11**, for which lipophilicity values were not determinable due to their poor solubility, all of the other compounds displayed good lipophilic-hydrophilic balance, with $logD^{7.4}$ values that were more favorable than that of reference compound **1**; values were in the range 2.2 – 2.6, which is optimal for favorable pharmacokinetic behavior. The difference between the logP value calculated for the neutral form (CLOGP), and the measured $logD^{7.4}$ value is in agreement with their being a significant amount of compound in the ionized form at physiological pH.

2.3 AKR1C3 and AKR1C2 inhibitor screening

The selective targeting of AKR1C3 over C2 is considered critical to effective PC therapy.[41] Not only do the two isoforms share 86% sequence similarity, but AKR1C2 is also involved in DHT inactivation, meaning that its inhibition is undesirable. Accordingly, the inhibitory potencies of compounds **3-13** were determined for both AKR1C2 and C3 and compared with that of ASP9521[27] and **1** (Table 1). Given the high sequence identity (97%) of AKR1C2 with C1 any inhibitory effects against C2 will be recapitulated against C1 and hence decided not to explore the latter isoform. Furtermore, the sequence and structural differences observed at the binding site between AKR1C3 and C4 hamper the possibility of the compounds to have an effect on AKR1C4, hence excluded the C4 isoform in this investigation aimed critically at understanding the C3 *vs* C2 selectivity ratio. IC_{50} was obtained using recombinant purified enzymes and by measuring S-tetralol oxidation in the presence of $NADP^+$. Except for compound **12**, which displayed an IC_{50} value that was five-times higher than that of compound **1**, all of the new compounds showed similar activity to **1** or better. Furthermore, the increased C3 *vs* C2 selectivity suggests that the active site of the C3 isoform can accommodate very bulky substituents, such as substituted or unsubstituted phenyl rings. Specifically, the incorporation of a phenyl substituent at the meta position of the aniline moiety (compound **5**) provided the most potent inhibition, as this modulation was responsible for a 4.5-fold increase in inhibitory activity. Indeed, **5** showed an IC_{50} value of 0.069 μM towards C3 and more than 1500-fold selectivity over C2. With respect to the activity of reference ASP9521, compound **5** was shown to exhibit similar potency under the conditions investigation but importantly with a higher C3 *vs* C2 selectivity (AKR1C3 IC_{50} = 0.044 μM ± 0.0025, 34.81% ± 2.95 of AKR1C2 inhibition at 20 μM). Although **4** presented IC_{50} values (IC_{50} 0.47 μM) in a similar range as reference **1**, its fluorescent properties hampered measurements of C2 inhibition at 100 μM. On the other hand, the phenoxy

substituent on the aniline moiety seems to slightly improve activity when inserted at the meta rather than the para position. For instance, meta-substituted compound **11** showed potent AKR1C3 inhibition, with an IC_{50} value of 0.11 μM, and more than 400-fold selectivity for C3 over C2, whereas para-substituted compound **10** displayed an IC_{50} of 0.27 μM and >370-fold selectivity. However, it is worth noting that both the meta and para methoxy-substituted derivatives **8** and **9** are equipotent with respect to AKR1C3 (IC_{50} of 0.22 μM and 0.26 μM, respectively), but are equally selective in targeting C3 over C2. Unexpectedly, the meta and para hydroxy-substituted derivatives **6** and **7** exhibit the same behavior as their methoxy precursors. The substitution of the triazole ring of derivative **5** with isoxazole, as in derivative **13**, represents a successful scaffold-hopping drug-design strategy, as demonstrated by the maintenance of activity towards AKR1C3 and the C3 *vs* C2 selectivity ratio. The slight decrease in activity towards the C3 isoform demonstrates that the triazole ring has better affinity for the active site of AKR1C3 than the isoxazole. However, the replacement was retained favorable as isoxazole **13** is more soluble than its triazole analogue **5** (see Table 2).

Table 1. Inhibitory effect of compounds **1** and **3-13** against the AKR1C3 and AKR1C2 recombinant purified enzymes.

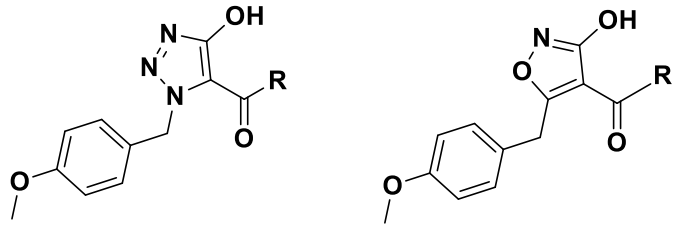

Compound	Structure	R =	AKR1C3 IC_{50}±SE (μM)	AKR1C2 % of inhibition at 100 μM
1 (hit)	A	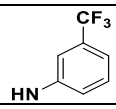	0.31 ± 0.01	59.89% ± 5.53
3	A	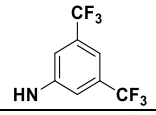	0.40 ± 0.027	33.57% ± 3.86
4	A	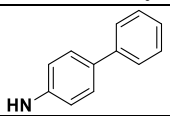	0.47 ± 0.020	30.0% ± 8.99[a] [at 20 μM]
5	A	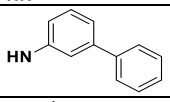	0.069 ± 0.0035	30.46% ± 6.81
6	A	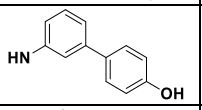	0.31 ± 0.037	37.93% ± 4.2
7	A	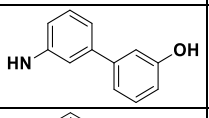	0.21 ± 0.016	38.55% ± 2.94
8	A	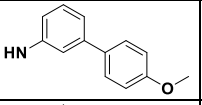	0.22 ± 0.022	31.57% ± 6.02[a] [at 50 μM]
9	A	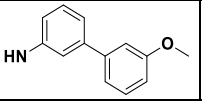	0.26 ± 0.078	45.27% ± 3.72

10	A	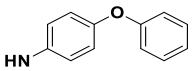	0.27 ± 0.024	57.82% ± 1.73
11	A	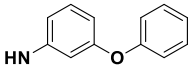	0.11 ± 0.0095	72.75% ± 0.29
12	A	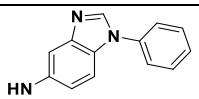	1.63 ± 0.13	-
13	**B**	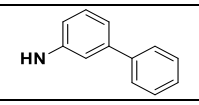	0.19 ± 0.023	7.32% ± 3.95

[a]The fluorescence properties of these compounds prevents measurements at 100 µM. The reported percentage of inhibition was measured at the dose indicated in brackets.

2.4 Inhibition of cell proliferation and PSA expression

The effects of the compounds on cell proliferation were evaluated using the 22RV1 PC cell line, which present high AKR1C3 expression.[25] The antiproliferative activity of the compounds was investigated by assessing cell viability using the sulforhodamine B (SRB) assay, and the IC_{50} values are reported in Table 2. Except for compound **12**, all of the other ligands exhibited a more pronounced antiproliferative effect than reference **1**.

The activity trend presented by the compounds on 22RV1 cells does not fully reflect the IC_{50} observed in inhibiting the enzyme. The most active compound on 22RV1 is **3** (IC_{50} = 33.80 µM); notably, it has the most favorable ligand-lipophilicity efficiency (LLE = 3.93) and the smallest substituent. To follow, inside the biphenylic triazolo derivatives, compounds **8** and **5** present the best IC_{50} values (50.10 and 52.06 µM respectively). The more flexible phenoxy substitution gave slightly lower activity both for the modulation of the para and that of the meta position, as demonstrated by the IC_{50} value of compounds **10** (58.18 µM) and **11** (64.95 µM). ASP9521 was tested in the same conditions and, at the concentration 50 µM, showed only 16 % of antiproliferative activity. Therefore compounds **3, 5** and **8** exhibited a more pronounced antiproliferative effect than ASP9521 in this cell model. Finally, scaffold hopping between the triazole and isoxazole maintained cellular activity (compare derivatives **5** and **13**), as well as lipophilicity, while increasing solubility and acidity, as previously described.

Table 2: Evaluation of the antiproliferative activity (IC_{50}) of compounds **1** and **3-13** using prostate cancer cell line 22rv1 (using the SRB assay), solubility and comparison of the measured $logD^{7.4}$ and CLOGP. For two selected compounds (**7** and **13**), pK_a value was measured; ligand-lipophilicity efficiency (LLE) is reported when calculable.

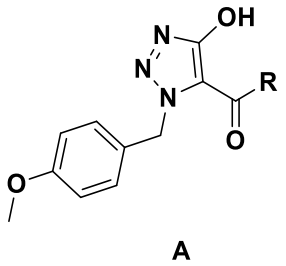

A

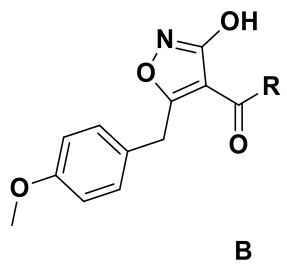

B

Compound	**Structure**	**R =**	**22RV1 IC_{50}±SE (µM)**	**Solubility in PBS (µM)**	**$logD^{7.4}$±SE (pKa)**	**CLOGP[d]**	**LLE[e]**

1 (hit)	A	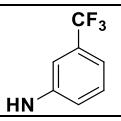	81.40 ± 2.29	21.2	1.10 ± 0.21	3.87	5.41
3	A	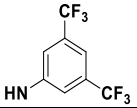	33.80 ± 0.68	6.91	2.47 ± 0.06	4.90	3.93
4	A	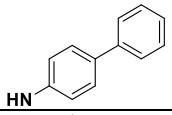	57.94 ± 1.23	<1[a]	2.19 ± 0.07	4.63	4.14
5	A	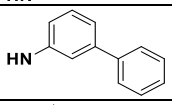	52.06 ± 0.99	<1[a]	2.30 ± 0.03	4.63	4.86
6	A	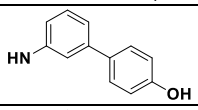	67.54 ± 1.94	2.05	2.19 ± 0.08	3.97	4.32
7	A	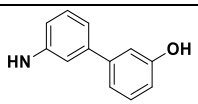	75.74 ± 0.91	40.33	2.25 ± 0.05 (4.9, 10.6)[c]	3.97	4.43
8	A	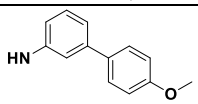	50.10 ± 0.81	<1[a]	2.59 ± 0.09	4.56	4.07
9	A	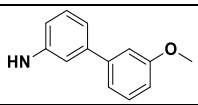	59.01 ± 0.94	<1[a]	2.50 ± 0.05	4.56	4.09
10	A	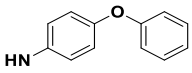	58.18 ± 1.01	<1[a]	n.d.[b]	4.54	-
11	A	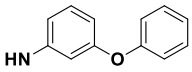	64.95 ± 1.67	<1[a]	n.d.[b]	4.54	-
12	A	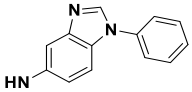	> 100 (36.88 % ± 4.37 at 100 μM)	1.25	2.19 ± 0.08	4.47	3.60
13	B	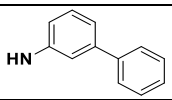	54.81 ± 2.47	10.75	2.16 ± 0.02 (4.5)[c]	6.26	4.56

[a] the value is lower than the limit of detection (LOD = 1 μM); [b] not determined because of low solubility in the water phase [c] measured adding different % of MDM to the medium (see Experimental part) on a Syrius T3 Instrument by CASSMedChem; [d] calculated using Bio-Loom for Windows, vers. 1.4 (BioByte Corp, Claremont, CA U.S.A); [e] calculated as LLE = $pIC_{50} - logD^{7.4}$, according to Murray *et al.[42]*

In order to assess the impact of therapeutically intervene on the steroidogenic pathway via AKR1C3 inhibition, the most potent C3 selective inhibitors (derivatives **5** and **11**, see Table 1) were evaluated for their potential to reduce prostate-specific antigen (PSA) expression in 22RV1 cells. Besides high AKR1C3-expression, this cell line also secretes PSA. Cells were incubated with compounds **5** and **11** at two different concentrations, selected at approximately the IC_{50} value of the antiproliferative activity and a ten-fold less concentration (50 μM and 5 μM, respectively). Then, the viable cells were lysed and the PSA levels were detected using western blot. Beta-actin was also included as a protein loading control in each lane. The western blot was quantified densitometrically and the PSA/β-actin values were calculated as fold change on the blot (Figure 7). As shown, PSA expression in the cell extracts was reduced when the cells were treated with both compounds. A relevant effect was also observed at 5 μM, the lowest concentration tested. These results confirm that both compounds inhibit prostate cancer cell proliferation through suppression of androgen synthesis by AKR1C3 inhibition.

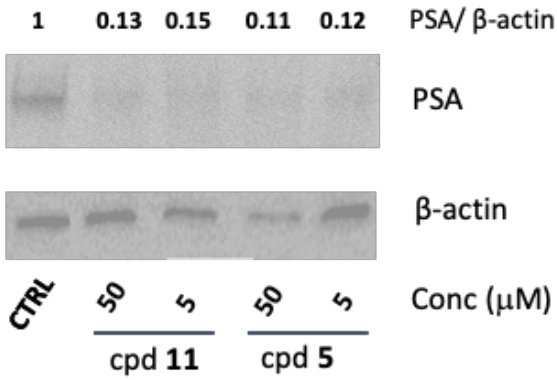

Figure 7. Inhibition of PSA expression on 22RV1 cells. The western blot analysis was performed on cell extracts of 22RV1 cultures incubated for 72 h with cpds **11** and **5** at two different concentrations (5 and 50 μM). PSA/β-actin values are calculated as fold change. The experiment was performed in duplicate.

To evaluate any possible enhanced effect that may occur with currently used drugs, compounds **5** and **11** were explored in combination with ABI and ENZA. The assays were carried out on the 22RV1 cell line, which has shown relative levels resistance to both ABI and ENZA.[7, 43, 44] Cells were incubated for 72 h with **5** or **11** at two different concentrations (40 and 60 μM) in the presence of either 10 μM ABI (Figure 8a), 30 μM ENZA (Figure 8b), or in the absence of drugs.
When compounds **5** or **11** were added together with ABI, cell viability was reduced by approximately 20% more than when using either drug alone, indicating an enhanced effect. This viability reduction was observed at both concentrations, albeit with slight differences for compound **5**.
A similar trend, but with increased effects, was observed by co-administrating both compounds with ENZA. In these cases, both **5** and **11** showed a reduction in cell viability by 30% and 50%, respectively, compared with either drug alone. These preliminary results are encouraging and may suggest the effectiveness of the combination therapy with known CRPC drugs. In particular these combination experiments confirm the potential of using an AKR1C3 inhibitor to therapeutically intervene key steps in the steroidogenic pathway and reduce resulting PSA production and cell tumor proliferation.

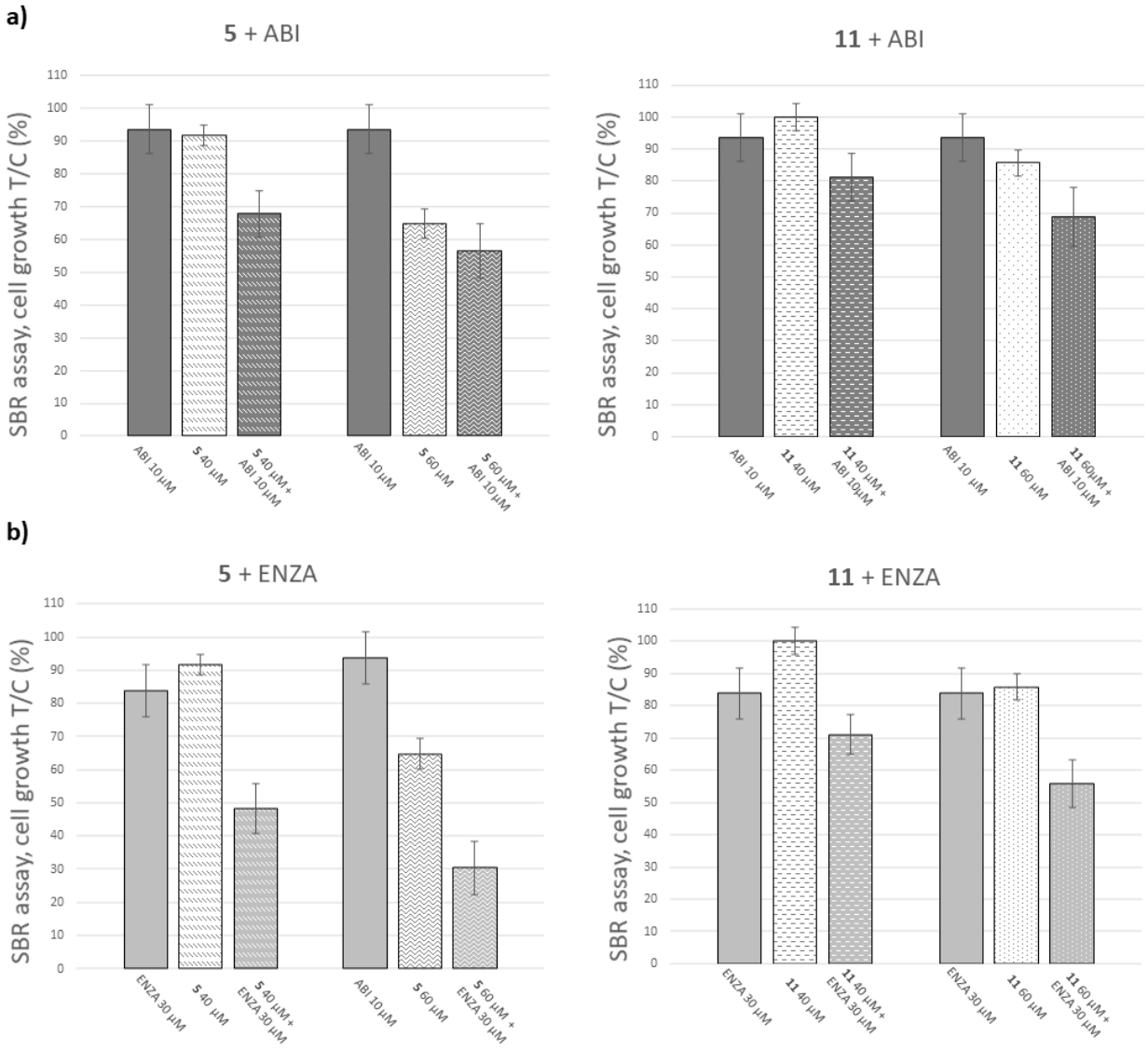

Figure 8. The effect of the co-treatment of compounds **5** and **11** with ABI (a) and ENZA (b) on 22RV1 cell proliferation, using the SRB assay. Cells were either treated with compounds **5** or **11** at 40 and 60 µM in the presence of a drug (10 µM ABI or 30 µM ENZA) or in the absence of a drug for 72 h. Cell growth is expressed as % T/C (mean OD of treated cells/mean OD of control cells X 100).

2.5 Inhibition of testosterone production in 22RV1 cells

As AKR1C3 plays a key role in the production of testosterone in the androgen biosynthetic pathway, the most potent AKR1C3 inhibitor, compound **5**, was also evaluated for its ability to interfere with testosterone formation in a cell-based system. The chosen assay better mimics a physiological environment than homogenate and purified enzyme-based assays. The formation of testosterone was analyzed in the cell supernatant by ELISA after AKR1C3-expressing 22RV1 cells were treated with compound **5** and androstenedione (AD). In the presence of only AD, testosterone production increased about 150-fold (Figure 9). When the cells were pre-treated with **5**, a significant dose-dependent impact on testosterone levels was observed (Figure 9). Testosterone production underwent a ca. 50-fold reduction when **5** was used at 50 µM, while 20% inhibition was detected when this analog was used at the 0.5 µM concentration, indicating a dose-dependent effect.

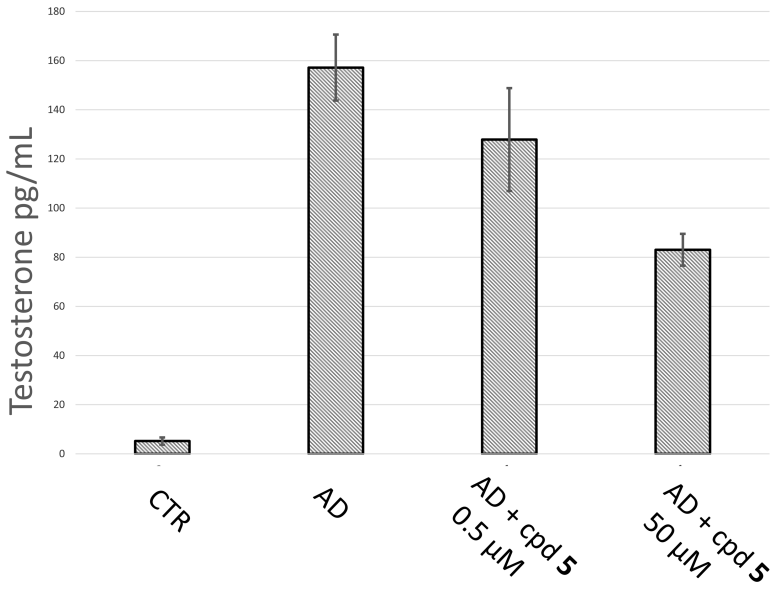

Figure 9. Inhibition of testosterone production. Evaluation of the inhibitory effect of compound **5** at two different concentrations (50 and 0.5 μM) in AD-treated 22RV1 cells.

3. Conclusions

This study has focused on a new series of AKR1C3 inhibitors that has been designed via structure-guided lead optimization on the 4-hydroxy-1-*p*-methoxybenzylazole scaffold, which previously led to the development of potent C3 *vs* C2 selective inhibitors. The introduction of a second phenyl substituent onto the aniline substructure of the lead compound improved both AKR1C3 potency and C3 *vs* C2 isoform selectivity, bringing this carboxyl acid-free hydroxytriazole series to reach activity values comparable to the best derivatives of AKR1C3 described in the literature. Compound **5**, bearing the phenyl substituent in the meta position of the aniline moiety, is the most potent compound against the isolated enzyme. Its modulation appeared to be responsible for the 4.5-fold increase in activity over reference compound **1**. Specifically, **5** shows nanomolar activity against AKR1C3, 1500-fold selectivity for C3 over C2 and is able to inhibit the cell proliferation of AKR1C3-expressing 22RV1 prostate cancer cells as well as inhibiting PSA expression. Compound **5** also has an effect on testosterone production in a dose-dependent manner. In addition, the inhibition of AKR1C3 activity by compounds **5** and **11** has been shown to have enhanced effects in combination with ENZA and ABI treatment suggesting the effectiveness of the combination therapy with these elective drugs to increase their efficacy. Overall, the novel small molecules reported provide a promising starting point for the design of more potent AKR1C3 inhibitors with clinical potential, which are essential for effective interventions in critical steps of the steroidogenic pathway and for reducing both PSA and testosterone production. The substitution of the triazole ring (compound **5**) with an isoxazole (compound **13**) is a successful scaffold-hopping drug-design strategy. This is supported by the facts that AKR1C3 activity is maintained, selectivity over AKR1C2 is increased and isoxazole **13** is more soluble than its triazole analogue **5**. Finally, the physicochemical characterization of the new library of analogs reported here, including pK_a, logD and solubility, will facilitate further optimization of these lead compounds, with the aim of discovering new compounds with improved drug-like properties and optimal pharmacokinetic characteristics.

4. Experimental section

4.1 Molecular Modeling

The structure of AKR1C3 complexed with compound **1** (PDB ID 6f2u[31]) was used to rationally design the new compounds and to perform *in-silico* simulations. Prior to docking studies, the protein was prepared by adding hydrogens and keeping the NADP+ cofactor. The designed compounds were sketched with moldraw and converted into mol2 using Open Babel;[45] their tautomeric/protonation state at physiological pH was checked using the MoKa software,[46] apart for the triazole hydroxyl group, which was considered to be deprotonated in accordance with experimental data.[26, 35, 47] Compounds were first minimized using a combination of the steepest descent and conjugate gradient minimization methods, and then submitted to docking with GOLD version 5.5.[48] The region of interest was defined to contain all of the residues within 10 Å of a reference residue, His117 (centroid of the docking cavity). An H-bond interaction between the NH of His117 and the deprotonated O atom of the hydroxyazole ring was applied as a constraint. The GOLD standard parameters were used and the complex subjected to 10 genetic algorithm runs. Finally, poses were scored with the CHEMPLP function and ranked accordingly.

Molecular dynamics simulations. The protein was parametrized by the Amber14 force field,[49] and Gromacs 5.1.4[50] was used to run MD Simulations. TIP3P was used as the water model. The solvated system was minimized using 5000 steps of steepest descent. The Verlet cutoff scheme, the Bussi−Parrinello thermostat LINCS for the constraints (all bonds), and the particle mesh Ewald for electrostatics, with a short-range cutoff of 11 Å, were applied. The system was equilibrated in four subsequent steps: 500 ps in the NVT ensemble at 100, 200 and 300 K, and 1 ns in the NPT ensemble, to reach the pressure equilibrium condition. In the two first equilibration steps, harmonic positional restraints were applied to the backbone of the protein with a spring constant of 1000 kJ/(mol·Å2). The production run was carried out in the NVT ensemble at 300 K without any restraint for 200 ns, at an integration step of 2 fs. MD setup and trajectory cleaning were performed using the BiKi LifeScience environment.[51, 52] The ligand was parameterized using the *ab-initio* RESP-charge-fitting methodology, as implemented in the BiKi Life Science software suite,[53] and converted into the GROMACS format using the acypipe tool.

The analyses of the MD trajectories were performed on the GROMACS package, and images were generated using PyMOL (Schrodinger, LLC. 2010. The PyMOL Molecular Graphics System, version 2.3.4).

4.2 Chemistry

General methods

All chemical reagents were obtained from commercial sources (Sigma Aldrich, Alfa Aesar) and used without further purification. ASP9521 was purchased by Vinci-Biochem. Culture media were obtained from Sigma‑Aldrich. Analytical grade solvents (acetonitrile, diisopropyl ether, diethyl ether, dichloromethane [DCM], dimethylformamide [DMF], ethanol 99.8 % v/v, ethyl acetate, methanol [MeOH], petroleum ether b.p. 40 - 60°C [petroleum ether]) were used without further purification. When needed, solvents were dried on 4 Å molecular sieves. Tetrahydrofuran (THF) was distilled immediately prior to use from Na and benzophenone under N_2. Thin layer chromatography (TLC) on silica gel was carried out on 5 x 20 cm plates with 0.25 mm layer thickness to monitor the progress of the reactions. Anhydrous $MgSO_4$ was used as a drying agent for the organic phases. Compound purification was achieved using flash column chromatography on silica gel (Merck Kieselgel 60, 230-400 mesh ASTM) and the indicated eluents. Purity was checked using two HPLC analytical methods, performed on a UHPLC chromatographic system (Perkin Elmer, Flexar). The analytical column was a UHPLC XBridge BEH C18 XP Column (2.1x100 mm, 2.5 µm particle size)

(Waters). Compounds were dissolved in acetonitrile and injected through a 20 µl loop. The mobile phase consisted of acetonitrile / water with 0.1 % trifluoroacetic acid. UHPLC analyses were run at flow rates of 0.5 mL/min, and the column effluent was monitored at 230 and 254 nm, referenced against a 400 nm wavelength. The purity of the final compounds was at least 95%. Melting points (m.p.) were measured on a capillary apparatus (Büchi 540) by placing the sample at a temperature 10° C below the m.p. and applying a heating rate of 2° C min^{-1}. All compounds were routinely checked by ^{1}H- and ^{13}C-NMR and mass spectrometry, except for compound **20**, which was only confirmed using mass (the presence of more than 2 tautomers makes the correct interpretation of NMR spectra difficult). ^{1}H- and ^{13}C-NMR spectra were performed on a JEOL ECZR600 instrument. The following abbreviations are used for coupling patterns: br = broad, s = singlet, d = doublet, dd = doublet of doublets, t = triplet, q = quartet, quint = quintuplet, m = multiplet. Chemical shifts (δ) are given in parts per million (ppm). The ^{1}H- and ^{13}C-NMR spectra of new compounds are shown in the supplementary data. MS spectra were performed on a Waters Micromass ZQ equipped with an ESCi source for electrospray ionization mass spectra (ESI). The HRMS spectra of the final compounds (compounds **3 - 12**) were recorded on a LTQ Orbitrap XL plus (Thermo Fisher Scientific, Waltham, MA USA) equipped with an ESI ionization source, with positive or negative ions (Spray capillary voltage: 3000 V (+), 2500 V (-)). Compound **14**,[37, 47, 54-56] was prepared by following previously described procedures.

*4'-(Benzyloxy)-[1,1'-biphenyl]-3-amine (**19**).* K_2CO_3 (3.35 g, 24.3 mmol) was added to a solution of 4-bromophenol **17** (17.3 mmol, 3.00 g) in dry acetonitrile, and the mixture was then stirred for 30 minutes. Benzyl bromide (17.3 mmol, 2.06 mL) was added and the resulting mixture was stirred overnight. The mixture was filtered through celite and the solvent was evaporated. The resulting solid was triturated from hexane to give pure compound 1-(benzyloxy)-4-bromobenzene **18** (yield 50%). $Pd[(C_6H_5)_3P]_4$ (263 mg, 0.22 mmol, 0.20 equiv.) was added to a solution of **18** (300 mg, 1.14 mmol, 1.00 eq) and K_2CO_3 (945 mg, 6.84 mmol, 6.00 eq) in a dioxane/water mixture (8:2 v/v). After the resulting mixture was stirred under a nitrogen atmosphere for 1 h at rt, (3-aminophenyl)boronic acid (2.28 mmol, 2.0 eq) was added. The reaction mixture was heated at reflux under a nitrogen atmosphere for 4 hours, then it was cooled to room temperature, diluted with water and the mixture was extracted three times with EtOAc. The combined organic layers were dried over Na_2SO_4 and concentrated under reduced pressure. The crude product was purified by flash chromatography (eluent: petroleum ether/EtOAc 8/2 v/v and then DCM) to give aniline **19** as an oil (Yield 63%). ^{1}H NMR (600 MHz, DMSO-d_6): δ 5.14 (s, 2H), 5.88 (very br s, 2H), 6.60 (d, J = 7.4 Hz, 1H, 6.83 (d, J = 7.3 Hz, 1H), 6.87 (s, 1H), 7.16 – 7.04 (m, 3H), 7.36 – 7.33 (m, 1H), 7.41 (t, J = 7.5 Hz, 2H), 7.53 – 7.44 (m, 4H).

*General procedure for compounds **15 a-h** and **16 a-b***

Oxalyl chloride (2 eq) and a catalytic amount of dry DMF were added to a cooled (0 °C) solution of the carboxylic acid **14** (1 eq) in dry THF. The reaction was stirred for 1 h at room temperature under a nitrogen atmosphere. The solvent was evaporated under reduced pressure and the residue was dissolved in dry THF (this process was repeated three times). The resulting acyl chloride was dissolved in dry toluene and used without any further purification in the next step. The appropriate anilines (1 eq) and dry pyridine (3 eq) were added to the described solution. The reaction mixture was stirred overnight at 50 °C under a nitrogen atmosphere. After the reaction completed, the mixture was poured into 2 M HCl, the layers were separated and the aqueous phase was extracted twice with ethyl acetate. The combined organic layer was washed with brine, dried over Na_2SO_4 and the solvent was evaporated. The crude product was purified using flash chromatography.

N-([1,1'-Biphenyl]-4-yl)-4-(benzyloxy)-1-(4-methoxybenzyl)-1H-1,2,3-triazole-5-carboxamide ***(15a)***. Flash chromatography, eluent: petroleum ether / EtOAc 90/10 v/v, yield 96%. White solid (m.p. 154.2 - 154.7 °C). ^{1}H NMR (600 MHz, $CDCl_3$): δ 3.77 (s, 3H), 5.61 (s, 2H), 5.93 (s, 2H), 6.85 (d, *J* = 8.8 Hz, 2H), 7.33 (t, *J* = 7.34 Hz, 1H), 7.41-7.48 (m, 7H), 7.49-7.58 (m, 8H), 8.67 (s, 1H). ^{13}C NMR (151 MHz, $CDCl_3$): 53.96, 55.34, 73.15, 112.61, 114.09, 120.37, 126.93, 127.32, 127.49, 127.81, 128.54, 128.90, 129.0, 129.11, 130.24, 135.45, 136.61, 137.65, 140.43, 155.43, 158.41, 159.73. MS (ESI) 491.5 $[M + H]^+$.

N-([1,1'-Biphenyl]-3-yl)-4-(benzyloxy)-1-(4-methoxybenzyl)-1H-1,2,3-triazole-5-carboxamide ***(15b)***. Flash chromatography, eluent: petroleum ether / EtOAc 90/10 v/v, yield 65%. White solid (m.p. 146.3-147.0 °C). ^{1}H NMR (600 MHz, $CDCl_3$): δ 3.77 (s, 3H), 5.60 (s, 2H), 5.93 (s, 2H), 6.85 (d, *J* = 8.6 Hz, 2H), 7.31-7.58 (m, 16H), 8.73 (s, 1H). ^{13}C NMR (151 MHz, $CDCl_3$): 53.96, 55.38, 73.24, 112.68, 114.13, 118.64, 118.84, 123.54, 127.29, 127.53, 127.76, 128.61, 128.89, 129.07, 129.15, 129.69, 130.30, 135.50, 137.90, 140.54, 142.29, 155.50, 158.45, 159.77. MS (ESI) 491 $[M + H]^+$.

4-(Benzyloxy)-N-(4'-(benzyloxy)-[1,1'-biphenyl]-3-yl)-1-(4-methoxybenzyl)-1H-1,2,3-triazole-5-carboxamide ***(15c)***. Flash chromatography, eluent: gradient of petroleum ether / EtOAc / DCM 60/20/20 to DCM, yield 76%. White solid (m.p. 165.5-167.4°C). ^{1}H NMR (600 MHz, $CDCl_3$): δ 3.77 (s, 3H), 5.14 (s, 2H), 5.60 (s, 2H), 5.92 (s, 2H), 6.85 (d, *J* = 8.8 Hz, 2H), 7.05 (d, *J* = 8.7 Hz, 2H), 7.30 (d, *J* = 7.9 Hz, 1H), 7.35 (t, *J* = 7.7 Hz, 2H), 7.37-7.50 (m, 13H), 7.51-7.53 (m, 2H), 8.71 (s, 1H). ^{13}C NMR (151 MHz, $CDCl_3$): 53.95, 55.39, 70.26, 73.24, 112.73, 114.15, 115.28, 118.17, 118.28, 123.10, 127.57, 127.62, 128.19, 128.32, 128.61, 128.79, 129.06, 129.13, 129.65, 130.30, 133.30, 135.53, 137.05, 137.90, 141.83, 155.49, 158.45, 158.73, 159.79. MS (ESI) 597 $[M + H]^+$.

4-(Benzyloxy)-N-(4'-methoxy-[1,1'-biphenyl]-3-yl)-1-(4-methoxybenzyl)-1H-1,2,3-triazole-5-carboxamide ***(15d)***. Flash chromatography, eluent: petroleum ether / EtOAc 90/10 v/v, yield 81%. White solid (m.p. 151.3-152.8 °C). ^{1}H NMR (600 MHz, $CDCl_3$): δ 3.77 (s, 3H), 3.87 (s, 3H), 5.60 (s, 2H), 5.93 (s, 2H), 6.85 (d, *J* = 8.8 Hz, 2H), 6.98 (d, *J* = 8.8 Hz, 2H), 7.31 (d, *J* = 7.8 Hz, 1H), 7.35 (t, *J* = 7.8 Hz, 1H), 7.57-7.38 (m, 11H), 8.70 (s, 1H). ^{13}C NMR (151 MHz, $CDCl_3$): 53.95, 55.38, 55.52, 73.23, 112.73, 114.15, 114.32, 118.19, 118.28, 123.11, 127.57, 128.31, 128.60, 129.06, 129.12, 129.64, 130.30, 133.07, 135.54, 137.89, 141.89, 155.50, 158.45, 159.54, 159.79. MS (ESI) 521 $[M + H]^+$.

4-(Benzyloxy)-N-(3'-methoxy-[1,1'-biphenyl]-3-yl)-1-(4-methoxybenzyl)-1H-1,2,3-triazole-5-carboxamide ***(15e)*** Flash chromatography, eluent: petroleum ether / EtOAc 80/20 v/v, yield 85%. White solid (m.p. 99.2-100.7 °C). ^{1}H NMR (600 MHz, $CDCl_3$): δ 3.77 (s, 3H), 3.88 (s, 3H), 5.60 (s, 2H), 5.92 (s, 2H), 6.85 (d, *J* = 8.7 Hz, 2H), 6.92 (dd, *J* = 8.2, 2.5 Hz, 1H), 7.07-7.09 (m, 1H), 7.12 (d, *J* = 7.7 Hz, 1H), 7.28-7.49 (m, 8H), 7.52 (m, 2H), 7.55 (d, *J* = 7.9, 2H), 8.71 (s, 1H). ^{13}C NMR (151 MHz, $CDCl_3$): 53.97, 55.38, 55.49, 73.26, 112.70, 112.92, 113.28, 114.15, 118.73, 119.06, 119.83, 123.60, 127.56, 128.58, 129.08, 129.19, 129.65, 129.89, 130.30, 135.50, 137.88, 142.12, 142.20, 155.51, 158.46, 159.79, 160.08. MS (ESI) 521 $[M + H]^+$.

4-(Benzyloxy)-1-(4-methoxybenzyl)-N-(4-phenoxyphenyl)-1H-1,2,3-triazole-5-carboxamide ***(15f)***. Flash chromatography, eluent: petroleum ether / EtOAc 90/10 v/v, yield 92%. White solid (m.p. 110.9-111.5 °C). ^{1}H NMR (600 MHz, $CDCl_3$): δ 3.77 (s, 3H), 5.59 (s, 2H), 5.91 (s, 2H), 6.84 (d, *J* = 8.7 Hz, 2H), 6.89-7.03 (m, 4H), 7.10 (t, *J* = 7.4 Hz, 1H), 7.33 (t, *J* = 8.0 Hz, 2H), 7.35-7.47 (m, 7H),

7.50 (d, J = 7.0 Hz, 2H), 8.57 (s, 1H). ^{13}C NMR (151 MHz, $CDCl_3$): 53.98, 55.38, 73.16, 112.58, 114.11, 118.63, 119.79, 121.83, 123.33, 127.54, 128.56, 129.02, 129.14, 129.88, 130.27, 132.77, 135.47, 153.95, 155.43, 157.52, 158.43, 159.76. MS (ESI) 507 $[M + H]^+$.

4-(Benzyloxy)-1-(4-methoxybenzyl)-N-(3-phenoxyphenyl)-1H-1,2,3-triazole-5-carboxamide ***(15g)***. Flash chromatography, eluent: petroleum ether / EtOAc 90/10 v/v, yield 93%. White solid (m.p. 113.3-114.2 °C). ^{1}H NMR (600 MHz, $CDCl_3$): δ 3.76 (s, 3H), 5.56 (s, 2H), 5.87 (s, 2H), 6.72 (d, J = 7.9 Hz, 1H), 6.82 (d, J = 8.4 Hz, 2H), 7.00 (d, J = 7.9 Hz, 2H), 7.08-7.66 (m, 13H), 8.58 (s, 1H). ^{13}C NMR (151 MHz, $CDCl_3$): 53.99, 55.37, 73.18, 110.95, 112.55, 114.10, 114.84, 114.97, 119.02, 123.56, 127.46, 128.48, 129.0, 129.13, 129.90, 130.24, 130.28, 135.38, 138.78, 155.41, 157.06, 157.86, 158.42, 159.76. MS (ESI) 507 $[M + H]^+$.

4-(Benzyloxy)-N-(3-bromophenyl)-1-(4-methoxybenzyl)-1H-1,2,3-triazole-5-carboxamide ***(15h)***. Flash chromatography, eluent: petroleum ether / EtOAc 80/20 v/v, yield 95%. White solid (m.p. 125.5-128.0°C). ^{1}H NMR (600 MHz, $CDCl_3$): δ 3.77 (s, 3H), 5.59 (s, 2H), 5.89 (s, 2H), 6.85 (d, J = 8.8 Hz, 2H), 7.15 (t, J = 8.0 Hz, 1H), 7.24 (ddd, J = 7.9, 1.8, 0.9 Hz, 1H), 7.28 (ddd, J = 8.1, 2.0, 0.9 Hz, 1H), 7.38-7.47 (m, 5H), 7.50 (dd, J = 7.9, 1.5 Hz, 2H), 7.70 (t, J = 2.0 Hz, 1H), 8.61 (s, 1H). ^{13}C NMR (151 MHz, $CDCl_3$): 54.05, 55.39, 73.36, 112.45, 114.17, 118.38, 122.86, 122.92, 127.39, 127.73, 128.59, 129.09, 129.28, 130.24, 130.49, 135.40, 138.72, 155.44, 158.53, 159.82. MS (ESI) 493 $[M + H]^+$.

4-(Benzyloxy)-N-(3,5-bis(trifluoromethyl)phenyl)-1-(4-methoxybenzyl)-1H-1,2,3-triazole-5-carboxamide ***(16a)***. Flash chromatography, eluent: petroleum ether / EtOAc 85/15 v/v, yield 68%. White solid (m.p. 151.2 – 153.0 °C). ^{1}H NMR (600 MHz, $CDCl_3$): δ 3.76 (s, 3H), 5.59 (s, 2H), 5.88 (s, 2H), 6.85 (d, J = 8.6 Hz, 2H), 7.49-7.39 (m, 5H), 7.48-7.55 (m, 2H), 7.59 (s, 1H), 7.86 (s, 2H), 8.92 (s, 1H). ^{13}C NMR (151 MHz, $CDCl_3$): 54.17, 55.40, 73.73, 112.09, 114.22, 117.86, 119.40, 123.05 (q, J = 272.5 Hz), 127.10, 128.61, 129.19, 129.55, 130.24, 132.61 (d, J = 33.4 Hz), 135.19, 139.00, 155.62, 158.80, 159.91. MS (ESI) 549 $[M - H]^-$.

4-(Benzyloxy)-1-(4-methoxybenzyl)-N-(1-phenyl-1H-benzo[d]imidazol-5-yl)-1H-1,2,3-triazole-5-carboxamide ***(16b)***. Flash chromatography, eluent: petroleum ether / EtOAc 70/30 v/v, yield 65%. White solid (m.p. 197.3-198.1°C). ^{1}H NMR (600 MHz, $CDCl_3$): δ 3.77 (s, 3H), 5.61 (s, 2H), 5.92 (s, 2H), 6.84 (d, J = 8.7 Hz, 2H), 7.35-7.56 (m, 12H), 7.58-7.63 (m, 2H), 8.05 (d, J = 1.5 Hz, 1H), 8.32 (s, 1H), 8.73 (s, 1H). ^{13}C NMR (151 MHz, $CDCl_3$): 54.02, 55.37, 73.18, 111.16, 111.49, 112.61, 114.09, 118.20, 124.15, 127.51, 128.61, 128.79, 129.07, 129.19, 130.37, 130.40, 130.64, 133.52, 135.45, 135.72, 142.28, 142.59. 155.58, 158.48, 159.74. MS (ESI) 531 $[M + H]^+$.

Procedure for synthesis of compounds ***3*** *and* ***4***

Protected compounds **16a** and **15a** (5 mmol) were separately dissolved in dry THF (10 mL) and hydrogenated in the presence of Pd/C (5% w/w) for 1 h at atmospheric pressure. The reaction mixture was filtered off through a short layer of celite and the solvent was evaporated under reduced pressure. The desired compound was then purified accordingly.

N-(3,5-bis(trifluoromethyl)phenyl)-4-hydroxy-1-(4-methoxybenzyl)-1H-1,2,3-triazole-5-carboxamide ***(3)***. The resulting solid was crystallized using acetonitrile. Yield 48%. (m.p. 223.1-225.1 °C). ^{1}H NMR (600 MHz, DMSO-d_6): δ 3.70 (s, 3H), 5.75 (s, 2H), 6.89 (d, J = 8.5 Hz, 2H),

7.24 (d, *J* = 8.4 Hz, 2H), 7.82 (s, 1H), 8.35 (s, 2H), 10.16 (s, 1H). ^{13}C NMR (151 MHz, DMSO-*d*$_6$): 53.25, 55.12, 110.80, 114.08, 116.98, 120.21, 123.21 (q, *J* = 272.8 Hz), 127.56, 129.36, 130.80 (q, *J* = 33.0 Hz), 139.88, 156.85, 158.62, 159.14. ESI−HRMS (m/z): $[M + H]^-$ calcd for $C_{19}H_{14}F_6N_4O_3$, 459.089733; obsd, 459.0897.

*N-([1,1'-biphenyl]-4-yl)-4-hydroxy-1-(4-methoxybenzyl)-1H-1,2,3-triazole-5-carboxamide (**4**).* The resulting solid was purified using flash chromatography, eluent: DCM / MeOH 98/2 v/v and subsequent crystallization (DCM / hexane). Yield 73%. White solid (m.p. 256.2-258.5°C). ^{1}H NMR (600 MHz, DMSO-*d*$_6$): δ 3.72 (s, 3H), 5.76 (s, 2H), 6.91 (d, *J* = 8.8 Hz, 2H), 7.27 (d, *J* = 8.8 Hz, 2H), 7.34 (t, *J* = 7.4 Hz, 1H), 7.46 (t, *J* = 7.8 Hz, 2H), 7.62 – 7.69 (m, 4H), 7.74 (d, *J* = 8.6 Hz, 2H), 9.98 (s, 1H). ^{13}C NMR (151 MHz, DMSO-*d*$_6$): 53.53, 55.61, 114.49, 120.62, 120.72, 126.82, 127.61, 127.68, 128.48, 129.46, 129.90, 136.0, 138.09, 140.08, 156.90, 159.55, 159.59. ESI−HRMS (m/z): $[M + H]^-$ calcd for $C_{23}H_{20}N_4O_3$, 399.1462; obsd, 399.1464.

*General procedure for compounds **5**, **6**, **8** – **12**.[57]*

The appropriate protected benzyloxytriazole (0.5 mol) was dissolved in TFA (2 mL), and thioanisole was added (3 mmol) at room temperature. The reaction mixture was stirred at room temperature for 2-3 h. After monitoring the disappearance of the starting material, the mixture was poured into water. When a precipitate was present, it was filtered off and washed with water and hexane. Otherwise, the aqueous mixture was extracted twice with ethyl acetate. The combined organic layer was washed with brine, dried over Na_2SO_4 and the solvent was evaporated. The crude product was further purified to give the corresponding final product.

*N-([1,1'-biphenyl]-3-yl)-4-hydroxy-1-(4-methoxybenzyl)-1H-1,2,3-triazole-5-carboxamide (**5**).* White solid (powder, m.p. 233.5-234.8 °C, from MeOH). Yield 63%. ^{1}H NMR (600 MHz, DMSO-*d*$_6$): δ 3.70 (s, 3H), 5.77 (s, 2H), 6.89 (d, *J* = 8.8 Hz, 2H), 7.26 (d, *J* = 8.7 Hz, 2H), 7.34 – 7.51 (m, 5H), 7.60 – 7.67 (m, 3H), 7.93 (s, 1H), 9.68 (broad s, 1H). ^{13}C NMR (151 MHz, DMSO-*d*$_6$): 53.17, 55.12, 111.22, 114.05, 118.22, 119.02, 122.55, 126.77, 127.73, 129.03, 129.43, 129.43, 129.59, 138.45, 139.91, 141.02, 156.21, 158.18, 159.12. ESI−HRMS (m/z): $[M + H]^-$ calcd for $C_{23}H_{20}N_4O_3$, 399.1462; obsd, 399.1463.

*4-Hydroxy-N-(4'-hydroxy-[1,1'-biphenyl]-3-yl)-1-(4-methoxybenzyl)-1H-1,2,3-triazole-5-carboxamide (**6**)*. The resulting solid was purified using flash chromatography, eluent: DCM / MeOH 95/5 v/v, and subsequent trituration with diisopropyl ether. White solid (powder, m.p. 239.0-244.2 °C). Yield 63%. ^{1}H NMR (600 MHz, DMSO-*d*$_6$): δ 3.71 (s, 3H), 5.78 (s, 2H), 6.87 (d, *J* = 8.6 Hz, 2H), 6.90 (d, *J* = 8.7 Hz, 2H), 7.27 (d, *J* = 8.7 Hz, 2H), 7.33 (d, *J* = 8.0 Hz, 1H), 7.39 (t, *J* = 7.9 Hz, 1H), 7.47 (d, *J* = 8.6 Hz, 2H), 7.55 (d, *J* = 8.0 Hz, 1H), 7.83 (s, 1H), 9.60 (s, 1H), 9.63 (broad s, 1H). ^{13}C NMR (151 MHz, DMSO-*d*$_6$): 53.14, 55.11, 111.23, 114.04, 115.78, 117.46, 117.98, 121.85, 127.72, 127.81, 129.41, 129.41, 130.59, 138.31, 141.03, 156.12, 157.32, 158.12, 159.10. ESI−HRMS (m/z): $[M + H]^-$ calcd for $C_{23}H_{20}N_4O_4$, 415.1412; obsd, 415.1413.

4-Hydroxy-N-(3'-hydroxy-[1,1'-biphenyl]-3-yl)-1-(4-methoxybenzyl)-1H-1,2,3-triazole-5-carboxamide (7). $Pd[(C_6H_5)_3P]_4$ (115 mg, 0.1 mmol, 0.20 eq) was added to a solution of **15h** (250 mg, 0.50 mmol, 1.00 eq) and K_2CO_3 (414 mg, 3.00 mmol, 6.00 eq) in a dioxane/water mixture (8:2 v/v). After the resulting mixture was stirred under a nitrogen atmosphere for 1 h at rt, (3-hydroxyphenyl)boronic acid (1.00 mmol, 2.0 eq) was added. The reaction mixture was heated at

reflux under a nitrogen atmosphere overnight, it was then cooled to room temperature and diluted with water, and the mixture was extracted three times with DCM. The combined organic layers were dried over Na_2SO_4 and concentrated under reduced pressure. The crude product was purified using flash chromatography (eluent: DCM / MeOH 95/5 v/v) and subsequent trituration with diisopropyl ether. White solid (powder, m.p. 196.0-197.7 °C). Yield 35 %. ^{1}H NMR (600 MHz, DMSO-*d*$_6$): δ 3.70 (s, 3H), 5.77 (s, 2H), 6.78 (ddd, *J* = 8.2, 2.4, 0.7 Hz, 1H), 6.90 (d, *J* = 8.8 Hz, 2H), 7.02 (t, *J* = 2.0 Hz, 1H), 7.05 (d, *J* = 8.2 Hz, 1H), 7.23-7.30 (m, 3H), 7.34 (d, *J* = 7.9 Hz, 1H), 7.41 (t, *J* = 7.9 Hz, 1H), 7.59 (d, *J* = 8.0 Hz, 1H), 7.90 (s, 1H), 9.57 (broad s, 1H), 9.82 (broad s, 1H). ^{13}C NMR (151 MHz, DMSO-*d*$_6$): 53.08, 55.10, 111.03, 113.49, 114.02, 114.70, 117.48, 117.98, 118.85, 122.28, 127.83, 129.37, 129.48, 130.01, 138.48, 141.11, 141.31, 156.33, 157.84, 158.75, 159.08. ESI−HRMS (m/z): $[M + H]^-$ calcd for $C_{23}H_{20}N_4O_4$, 415.1412; obsd, 415.1413.

*4-Hydroxy-N-(4'-methoxy-[1,1'-biphenyl]-3-yl)-1-(4-methoxybenzyl)-1H-1,2,3-triazole-5-carboxamide (**8**).* The resulting solid was purified using flash chromatography, eluent: DCM / MeOH 95/5 v/v, and subsequent trituration with diisopropyl ether. White solid (powder, m.p. 244.0-247.9°C). Yield 61%. ^{1}H NMR (600 MHz, DMSO-*d*$_6$): δ 3.70 (s, 3H), 3.79 (s, 3H), 5.77 (s, 2H), 6.89 (d, *J* = 8.8 Hz, 2H), 7.03 (d, *J* = 8.8 Hz, 2H), 7.26 (d, *J* = 8.7 Hz, 2H), 7.35 (d, *J* = 8.0 Hz, 1H), 7.40 (t, *J* = 7.8 Hz, 1H), 7.55 – 7.60 (m, 3H), 7.86 (s, 1H), 9.65 (s, 1H). ^{13}C NMR (151 MHz, DMSO-*d*$_6$): 53.14, 55.10, 55.20, 111.20, 114.03, 114.42, 117.67, 118.31, 122.03, 127.72, 127.82, 129.40, 129.46, 132.20, 138.37, 140.64, 154.25, 156.16, 158.17, 159.08. ESI−HRMS (m/z): $[M + H]^-$ calcd for $C_{24}H_{22}N_4O_4$, 429.1568; obsd, 429.1565.

*4-Hydroxy-N-(3'-methoxy-[1,1'-biphenyl]-3-yl)-1-(4-methoxybenzyl)-1H-1,2,3-triazole-5-carboxamide (**9**).* The resulting solid was purified using flash chromatography, eluent: DCM / MeOH 95/5 v/v, and subsequent trituration with EtOAc. White solid (powder, m.p. 178-181.4 °C). Yield 48%. ^{1}H NMR (600 MHz, DMSO-*d*$_6$): δ 3.71 (s, 3H), 3.83 (s, 3H), 5.78 (s, 2H), 6.90 (d, *J* = 8.7 Hz, 2H), 6.97 (dd, *J* = 8.2, 2.3 Hz, 1H), 7.16 – 7.18 (m, 1H), 7.21 (d, *J* = 7.8 Hz, 1H), 7.27 (d, *J* = 8.7 Hz, 2H), 7.39 – 7.46 (m, 3H), 7.65 (d, *J* = 7.5 Hz, 1H), 7.91 (s, 1H), 9.68 (s, 1H). ^{13}C NMR (151 MHz, DMSO-*d*$_6$): 53.16, 55.10, 55.18, 111.19,112.33, 113.18, 114.03, 118.34, 119.07, 119.19, 122.63, 127.70, 129.40, 129.48, 130.07, 138.34, 140.87, 141.41, 156.18, 158.08, 159.10, 159.75. ESI−HRMS (m/z): $[M + H]^-$ calcd for $C_{24}H_{22}N_4O_4$, 429.1568; obsd, 429.1565.

*4-Hydroxy-1-(4-methoxybenzyl)-N-(4-phenoxyphenyl)-1H-1,2,3-triazole-5-carboxamide (**10**).* The resulting solid was purified using flash chromatography, eluent: DCM / MeOH 95/5 v/v, and subsequent trituration with EtOAc. White solid (powder, m.p. 239.0-241.3 °C). Yield 58%. ^{1}H NMR (600 MHz, DMSO-*d*$_6$): δ 3.71 (s, 3H), 5.75 (s, 2H), 6.90 (d, *J* = 8.7 Hz, 2H), 6.99 (d, *J* = 7.8 Hz, 2H), 7.02 (d, *J* = 8.9 Hz, 2H), 7.12 (t, *J* = 7.4 Hz, 1H), 7.26 (d, *J* = 8.7 Hz, 2H), 7.41 – 7.35 (m, 2H), 7.65 (d, *J* = 8.9 Hz, 2H), 9.60 (br s, 1H). ^{13}C NMR (75 MHz, DMSO-*d*$_6$): 53.06, 55.12, 111.21, 114.02, 118.08, 119.48, 121.74, 123.19, 127.77, 129.40, 130.04, 133.64, 152.53, 155.97, 157.17, 158.22, 159.09. ESI−HRMS (m/z): $[M + H]^-$ calcd for $C_{23}H_{20}N_4O_4$, 415.1412; obsd, 415.1412.

*4-Hydroxy-1-(4-methoxybenzyl)-N-(3-phenoxyphenyl)-1H-1,2,3-triazole-5-carboxamide (**11**).* The resulting solid was purified using flash chromatography, eluent: DCM / MeOH 95/5 v/v, and subsequent crystallization (DCM / hexane). White solid (powder, m.p. 217.5-222.0 °C). Yield 75%. ^{1}H NMR (600 MHz, DMSO-*d*$_6$): δ 3.71 (s, 3H), 5.71 (s, 2H), 6.74 (d, *J* = 7.5 Hz, 1H), 6.88 (d, *J* = 8.6 Hz, 2H), 7.04 (d, *J* = 8.2 Hz, 2H), 7.16 (t, *J* = 7.0 Hz, 1H), 7.22 (d, *J* = 8.5 Hz, 2H), 7.30-7.36 (m, 2H), 7.37-7.46 (m, 3H), 9.75 (broad s, 1H). ^{13}C NMR (151 MHz, DMSO-*d*$_6$): 53.10, 55.11, 109.98, 111.09, 114.02, 114.79, 118.78, 123.64, 127.68, 129.38, 130.11, 130.31, 137.66, 139.48, 156.21,

156.45, 157.04, 158.46, 159.09. ESI−HRMS (m/z): $[M + H]^-$ calcd for $C_{23}H_{20}N_4O_4$, 415,1412; obsd, 415.1415.

*4-Hydroxy-1-(4-methoxybenzyl)-N-(1-phenyl-1H-benzo[d]imidazol-5-yl)-1H-1,2,3-triazole-5-carboxamide (**12**).* The resulting solid was subsequently crystallized from MeOH. White solid (powder, m.p. 240.1-243.7 °C). Yield 48%. ^{1}H NMR (600 MHz, DMSO-d_6): δ 3.71 (s, 3H), 5.79 (s, 2H), 6.91 (d, J = 6.7 Hz, 2H), 7.29 (d, J = 6.8 Hz, 2H), 7.47 (d, J = 8.8 Hz, 1H), 7.50 (d, J = 7.3 Hz, 1H), 7.58 – 7.66 (m, 3H), 7.69 (d, J = 7.3 Hz, 2H), 8.19 (s, 1H), 8.58 (d, J = 2.1 Hz, 1H), 9.69 (s, 1H). ^{13}C NMR (151 MHz, DMSO-d_6): 53.15, 55.12, 110.83, 111.11, 111,37, 114.03, 117.13, 117.21, 123.49, 127.77, 129.50, 129.92, 130.15, 133.07, 135.92, 143.96, 144.08, 156.02, 158.03, 159.12. ESI−HRMS (m/z): $[M + H]^-$ calcd for $C_{24}H_{20}N_6O_3$, 439.1524; obsd, 439.1525.

*Dimethyl 2-(2-(4-methoxyphenyl)acetyl)malonate (**20**).* Dimethyl malonate (1.74 g, 0.0132 mol, 1.0 equiv.) was added to a suspension of magnesium chloride (1.26 g, 0.0132 mol, 1.0 eq) in dry DCM (40 mL). The suspension was cooled to 0 °C and pyridine (2.13 mL, 0.0264 mol, 2.0 eq) was added. After stirring for 15 minutes, freshly obtained (from the corresponding acid) 2-(4-methoxyphenyl)acetyl chloride (2.44 g, 0.0132 mol, 1.0 eq) was slowly added, and the reaction mixture was stirred for one hour at 0 °C, and then allowed to stir at room temperature overnight. The reaction mixture was quenched in cooled 2 M HCl solution (100 mL) and the layers were separated. The aqueous layer was extracted with DCM (2x 700 mL). The combined organic layers were washed with brine, dried over Na_2SO_4 and concentrated under reduced pressure.

The crude product was purified using flash chromatography (eluent: petroleum ether / EtOAc 8/2 v/v) to give **20** as a pale yellow oil (yield 60%). MS (ESI) 303 $[M + Na]^+$, 319 $[M + K]^+$.

*Dimethyl 2-(1-methoxy-2-(4-methoxyphenyl)ethylidene)malonate (**21**).* K_2CO_3 (1.36 g, 9.83 mmol, 1.3 eq) was added to a solution of **20** (2.12 g, 7.56 mmol) in DMF (30 mL). After stirring for 20 minutes, dimethyl sulfate (0.932 mL, 9.83 mmol, 1.3 eq) was added dropwise and the mixture was stirred overnight. It was then quenched in saturated aq. NH_4Cl solution (100 mL) and extracted with EtOAc (3 x 100 mL). The combined organic phases were washed with brine, dried over Na_2SO_4 and concentrated under reduced pressure. The crude product was purified using flash column chromatography, eluent: petroleum ether / EtOAc 8/2 v/v, to give **21** as a white solid. M.p. 63.6 – 66.2 °C. Yield 48%. ^{1}H NMR (600 MHz, $CDCl_3$): δ 3.68 (s, 3H), 3.72 (s, 3H), 3.78 (s, 3H), 3.81 (s, 3H), 4.25 (s, 2H), 6.85 (d, J = 8.7 Hz, 2H), 7.17 (d, J = 8.7 Hz, 2H). ^{13}C NMR (151 MHz, $CDCl_3$): δ 32.64, 51.94, 55.40, 56.20, 108.52, 114.49, 126.96, 129.27, 158.64, 165.42, 167.02, 171.86. MS (ESI) 317 $[M + Na]^+$.

*Methyl 3-hydroxy-5-(4-methoxybenzyl)isoxazole-4-carboxylate (**22**).* A solution of sodium methoxide was prepared by treating sodium (0.352 g, 15.3 mmol, 3.0 eq, cut into small pieces) with methanol (10 mL). A solution of hydroxylamine hydrochloride (0.496 g, 7.14 mmol, 1.4 eq) in dry methanol (10 mL) and, subsequently, a solution of **21** (1.5 g, 5.10 mmol, 1.0 eq) in dry methanol (10 mL) were slowly added to the sodium methoxide solution at 0 °C. The reaction was allowed to warm to room temperature and was stirred overnight. The reaction was quenched into a saturated solution of NH_4Cl (50 mL), diluted with water and the pH was adjusted to pH 2 with 2 M HCl. The resulting white solid was washed with water to give isoxazole **22**. White solid (powder, m.p. 126.3 – 127.5 °C). Yield 69 %. ^{1}H NMR (600 MHz, $CDCl_3$): δ 3.72 (s, 3H), 3.77 (s, 3H), 4.25 (s, 2H), 6.88 (d, J = 8.6 Hz, 2H), 7.18 (d, J = 8.5 Hz, 2H), 11.90 (br s, 1H). ^{13}C NMR (151 MHz, $CDCl_3$): δ 32.07, 51.54,

55.08, 99.45, 114.14, 127.14, 129.87, 158.32, 16.45, 168.11, 177.80. MS (ESI) 264 $[M + H]^+$, 286 $[M + Na]^+$.

*Methyl 3-benzyloxy-5-(4-methoxybenzyl)isoxazole-4-carboxylate (**23**).* Ag_2O (0.897 g, 3.87 mmol, 1.5 equiv.) was added to a stirred solution of isoxazole **22** (0.680 g, 2.58 mmol, 1.0 equiv.) in DMF (10 mL). After stirring for 5 minutes, benzyl bromide (0.369 mL, 3.10 mmol, 1.2 equiv.) was added and the reaction mixture was shielded from the light with aluminum foil and stirred at room temperature for 2 hours. The reaction mixture was directly charged onto a flash chromatography column and eluted with petroleum ether / EtOAc (from 9/1 v/v to 7/3 v/v) to give **23** as a white solid. M.p. 89.0 – 90.8 °C. Yield 52 %. ^{1}H NMR (600 MHz, $CDCl_3$): δ 3.78 (s, 3H), 3.58 (s, 3H), 4.28 (s, 2H), 5.32 (s, 2H), 6.84 (d, *J* = 8.6 Hz, 2H), 7.23 (d, *J* = 8.6 Hz, 2H), 7.33 (t, *J* = 7.3 Hz, 1H), 7.38 (t, *J* = 7.4 Hz, 2H), 7.46 (d, *J* = 7.3 Hz, 1H). ^{13}C NMR (151 MHz, $CDCl_3$): δ 32.95, 51.87, 55.41, 71.80, 100.13, 114.30, 127.01, 127.94, 128.43, 128.65, 130.15, 135.77, 158.93, 161.83, 169.17, 178.62. MS (ESI) 354 $[M + H]^+$, 376 $[M + Na]^+$.

*3-(Benzyloxy)-5-(4-methoxybenzyl)isoxazole-4-carboxylic acid (**24**)*. 5 M NaOH (5.0 eq.) was added to a solution of **23** (0.706 g, 2 mmol, 1.0 eq) in methanol (20 mL). The solution was heated to 50°C and stirred overnight. It was then diluted with water (40 mL), acidified to pH 2 with 2N HCl. The resulting suspension was filtered and the solid was well washed with water to give the carboxylic acid **24**. Yield 89%. White solid (m.p. 185.4 – 186.6 °C). ^{1}H NMR (600 MHz, DMSO-*d*$_6$): δ 3.71 (s, 3H), 4.29 (s, 2H), 5.26 (s, 2H), 6.88 (d, *J* = 8.6 Hz, 2H), 7.19 (d, *J* = 8.6 Hz, 2H), 7.34 - 7.42 (m, 3H), 7.46 (d, *J* = 7.2 Hz, 2H). ^{13}C NMR (151 MHz, DMSO-*d*$_6$): δ 31.85, 55.06, 71.12, 100.24, 114.13, 127.16, 128.13, 128.30, 128.42, 129.79, 135.73, 158.31, 161.77, 168.77, 178.05. MS (ESI) 340 $[M + H]^+$.

*N-([1,1'-biphenyl]-3-yl)-3-(benzyloxy)-5-(4-methoxybenzyl)isoxazole-4-carboxamide (**25**).* Oxalyl chloride (0.202 mL, 2.36 mmol, 2.0 eq) and a catalytic amount of dry DMF were added to a cooled (0 °C) solution of the carboxylic acid **24** (0.40 g, 1.18 mmol, 1 eq) in dry THF (40 mL). The reaction was stirred for 1 h at room temperature under a nitrogen atmosphere. The solvent was evaporated under reduced pressure and the residue was dissolved in dry THF (this process was repeated three times). The resulting acyl chloride was dissolved in dry THF (40 mL), and 3-aminobyphenyl (0.200 g, 1.18 mmol, 1.0 eq) and dry pyridine (0.286 mL, 3.54 mmol, 3.0 eq) were added at 0° C. The reaction mixture was stirred overnight under a nitrogen atmosphere. After the reaction completed, the mixture was poured into 2 M HCl, and then extracted with EtOAc (3x100 mL). The combined organic layer was washed with brine, dried over Na_2SO_4 and the solvent was evaporated. The crude product was purified using flash chromatography, eluent: petroleum ether / EtOAc 8/2 v/v, to give **25** as a white solid (m.p. 141.3 – 145.9 °C). Yield 52 %. ^{1}H NMR (600 MHz, $CDCl_3$): δ 3.78 (s, 3H), 4.47 (s, 2H), 5.43 (s, 2H), 6.85 (d, *J* = 8.7 Hz, 2H), 7.41 – 7.32 (m, 5H), 7.50 – 7.42 (m, 5H), 7.55 – 7.50 (m, 5H), 7.60 – 7.55 (m, 1H), 8.64 (s, 1H). ^{13}C NMR (151 MHz, $CDCl_3$): δ 32.66, 55.34, 73.30, 101.49, 114.24, 118.49, 118.73, 123.20, 127.23, 127.37, 127.64, 128.62, 128.80, 129.11, 129.34, 129.60, 130.38, 134.86, 138.17, 140.54, 142.15, 158.40, 158.86, 167.22, 178.46. MS (ESI) 491 $[M + H]^+$.

*N-([1,1'-biphenyl]-3-yl)-3-hydroxy-5-(4-methoxybenzyl)isoxazole-4-carboxamide (**13**).* Protected compound **25** (0.230 g, 0.47 mmol) was dissolved in dry THF (30 mL) and hydrogenated in the presence of Pd/C (10% w/w) for 1 h at atmospheric pressure. The reaction mixture was filtered off through a short layer of celite and the solvent was evaporated under reduced pressure. The desired compound was then purified using flash chromatography, eluent: DCM / MeOH /HCOOH 98/2/0.1 v/v/v, to give isoxazole **13** as a white solid (m.p. 192.6 – 193.2 °C). Yield 74 %. ^{1}H NMR (600 MHz,

DMSO-d_6): δ 3.71 (s, 3H), 4.32 (s, 2H), 6.88 (d, J = 7.9 Hz, 2H), 7.24 (d, J = 7.8 Hz, 2H), 7.52 – 7.35 (m, 6H), 6.67 – 6.63 (m, 3H), 7.98 (s, 1H), 9.49 (br s, 1H). ^{13}C NMR (151 MHz, DMSO-d_6): δ 31.73, 55.06, 102.29, 114.10, 118.25, 119.03, 122.37, 126.74, 127.52, 127.66, 128.98, 129.47, 129.90, 138.61, 139.95, 140.93, 158.27, 158.92, 166.98, 176.06. ESI−HRMS (m/z): $[M + H]^+$ calcd for $C_{24}H_30N_2O_4$, 401.1496; obsd, 401.1498.

4.3. Physicochemical Characterization

4.3.1. Solubility assay. Solubility was determined in phosphate buffer saline (PBS, 50 mM, pH 7.4). Each solid compound (ca. 1 mg) was added to 1 mL of PBS and the resulting suspension was shaken at 25°C for 24 h. The suspensions were filtered through a PTFE 0.45µm filter (VWR), and the solutions were analyzed using UHPLC on a PerkinElmer ultrahigh performance liquid chromatography (UHPLC) instrument, equipped with a reverse-phase (RP) C18 XBridge BEH C18 XP Waters column (2.1x100mm, 2.5 µm particle size). Gradient elution: the ratio of eluents A and B (0.1% trifluoroacetic acid in water and 0.1% trifluoroacetic acid in methanol, respectively) changed linearly from 60% A − 40% B to 0% A − 100% B over 6 min, followed by 3 min in isocratic elution at 100% eluent B and then 4 min in equilibration elution to reset the starting conditions. The flow rate was 0.5 mL/min. The standard injection volumes were either 2, or 6 µL for poorly soluble compounds. The detection system was a PerkinElmer diode array detector. The column effluent was monitored at 254 and 230 nm, and referenced against a 600 nm wavelength. Solubility, expressed as the µM concentration of the saturated solution, was calculated via interpolation with external calibration curves, which were obtained with solutions of each compound in methanol (linearity determined in a concentration range of 1-200 µM; $r^2 > 0.99$).

4.3.2. Ionization and lipophilicity behavior. The ionization constants of the compounds were determined via potentiometric titration with the SiriusT3 apparatus (Sirius Analytical Instruments Ltd., East Sussex, UK) by CASSMedChem. All compounds required titration in the presence of a multicomponent cosolvent system containing polar and nonpolar solvents (20% ACN, 20% Dioxane, 20% MeOH), which is referred to as MDM. MDM was mixed with water as a cosolvent in variable amounts (52 % for **7**, 54% for **13**).

CLOGP values were calculated using the Bio-Loom program for Windows, version 1.4 (BioByte Corp, Claremont, CA U.S.A). The partition coefficients between *n*-octanol and PBS at pH 7.4 (log $D^{7.4}$) were obtained using the shake-flask technique at room temperature. In the shake-flask experiments, 50 mM of phosphate buffered saline at pH 7.4 (ionic strength adjusted to 0.15 M with KCl) was used as the aqueous phase. The organic and aqueous phases were mutually saturated via shaking for 4 h. The compounds were solubilized in the buffered aqueous phase at the highest concentration compatible with solubility, and appropriate amounts of *n*-octanol were added. The two phases were shaken for about 20 min, by which time the partitioning equilibrium of solutes had been reached, and then centrifuged (10000 rpm, 10 min). The concentration of the solutes was measured in the aqueous phase on a UV spectrophotometer (UV-2501PC, Shimadzu); absorbance values (recorded for each compound at the wavelength of maximum absorption) were interpolated in calibration curves obtained using standard solutions of the compounds (r^2 >0.99). Each log D value is an average of at least six measurements.

4.4 AKR1C3 and AKR1C2 inhibitor screening

The expression and purification of the AKR1C3 and AKR1C2 enzymes were performed as previously described.[25] Briefly, the bacteria cells were grown in YT2X media that was supplemented with ampicillin, and at OD600 nm = 0.6 the expression was induced by IPTG 0.5 mM for 2 h. The bacteria were then centrifuged and lysed with four freeze-thaw cycles in the presence of lysozyme and protease inhibitors. The lysate was centrifuged for 30 min at 13,000xg and the supernatant was

collected. AKR1C3 and AKR1C2 were affinity purified via N-terminal GST-tag on glutathione (GT) sepharose (GE-Healthcare) and cleaved by thrombin, according to the manufacturer's protocol.

The inhibition assays were performed on purified recombinant enzymes, as previously described.[25] Briefly, the enzymatic reaction was fluorimetrically (exc/em; 340 nm/460 nm) monitored by the measurement of NADPH production on a "Ensight" plate reader (Perkin Elmer) at 37° C. The assay mixture, which contained S-tetralol (in EtOH), the inhibitor (in EtOH), 100 mM phosphate buffer pH 7, 200 μM $NADP^+$ and purified recombinant enzyme (30 μl), was added to a 96-well plate at a final volume of 200 μl and 10% EtOH. The S-tetralol concentrations used in the AKR1C2 and AKR1C3 inhibition assays were 15 μM and 160 μM, respectively, in accordance with the Km described for the respective isoforms under the same experimental conditions. Percentage inhibition with respect to the controls that contained the same amount of solvent, without inhibitor, was calculated from the initial velocities, which were obtained via the linear regression of the progress curve at different inhibitor concentrations. The IC_{50} values were obtained using PRISM 7.0 GraphPad Software. Results are expressed as mean value ± standard error (SE) of at least three experiments, each carried out in triplicate.

4.5. Tumor cell cultures

Prostate cancer 22RV1 cells were maintained as monolayers in RPMI, which was supplemented with 10% (v/v) fetal calf serum, 2% (v/v) penicillin-streptomycin and 0.03% L-glutamine. Cells were grown at 37 °C in a humidified atmosphere containing 5% CO_2.

4.6. Cell proliferation assay

Cell growth inhibition was evaluated using a sulforhodamine B colorimetric proliferation assay (SRB assay) modified by Vichai and Kirtikara, as previously described.[25] Cells (10,000 cells/well for 22RV1) were seeded into 96-well plates in the specific medium containing 10% charcoal stripped serum, and incubated for 24 h. Various dilutions of inhibitors in DMSO were then added in triplicate, and incubated for 72 h. Control cells were incubated with the same final concentration of DMSO (maximum concentration 1% v/v).

For the co-treatment experiments, 22RV1 cells were treated with either ABI (10 μM) or ENZA (30 μM), with or without compounds **5** and **11**, at two different concentrations (40 and 60 μM) for 72 h.

The IC_{50} values were obtained using PRISM 7.0 GraphPad Software. The values are the mean of three separate experiments, each carried out in triplicate.

4.7. Western Blot

For the determination of PSA expression, 22RV1 cells (300,000 cells per well) were seeded into 6-well plates in the specific medium containing 10% charcoal stripped serum, and were incubated for 24 h. Two different dilutions of cpds **5** and **11** in DMSO were then added to the wells and incubated for 72 h.

Control cells were incubated with the same final concentration of DMSO (maximum concentration 0.5% v/v). Protein extraction from both untreated and treated cells was conducted using a RIPA lysis buffer containing the Complete Protease Inhibitor Cocktail (Roche Molecular Biochemicals). 30 μg of total protein lysate was loaded for analysis by western blot.

For the detection of PSA, a 1:500 dilution of mouse monoclonal anti-PSA (sc-7316 Santa Cruz Biotechnology) was prepared in blocking buffer, added to the membrane and incubated overnight at 4°C on a shaker. The membrane was washed with TBS and incubated with a HRP-conjugated

secondary anti-mouse antibody (Santa-Cruz Biotechnology), diluted 1:10000, for 2 h at room temperature on a shaker. Visualization was achieved using the chemiluminescent substrate Amersham ECL prime and captured using the ChemiDoc Imaging System (Biorad). Rabbit anti-β-actin (Cell Signaling Technology) was used as the internal control with a dilution of 1:1,000 in blocking buffer, with overnight incubation at 4°C on a shaker. For the detection of AKR1C3, a 1:5,000 dilution of mouse monoclonal anti-AKR1C3 (Sigma Aldrich) was used.

4.8. Inhibition of the AKR1C3-mediated production of testosterone in 22RV1 cells by Elisa

22RV1 cells were seeded into 96-well plates in the specific medium, which contained 10% charcoal stripped serum, at a density of 30,000 cells per well, and were incubated for 24 h. Cpd **5** was added to the wells at 2 different concentrations and incubated for 1 h. An equimolar (30 nM) concentration of androstenedione was then added to the wells. The plate was returned to the incubator for a further 24 h. The cell supernatant (dilution 1:2) was analyzed using a Testosterone Elisa Kit (Cayman Chemical Company), according to the manufacturer's guide. The ELISA plate was read at a wavelength of 405 nm on a microplate reader. Analysis was performed using the Cayman Chemical Company's online available analysis tool, and data was quantitated against a standard curve generated in ELISA buffer. The values are the mean of three separate experiments each carried out in triplicate.

Abbreviations used

Aldo-keto reductase C3 isoform (AKR1C3), prostate cancer (PC), androgen deprivation therapy (ADT), castration-resistant prostate cancer (CRPC), androgen receptor (AR), flufenamic acid (FLU), sub-pocket 2 (SP2), sub-pocket 1 (SP1), cyclooxygenase (COX), aldo-keto reductase C2 isoform (AKR1C2), hexadeuterodimethyl sulfoxide (DMSO-d6), deuterochloroform (CDCl3), prostatic serum antigen (PSA).

Author information

Corresponding Authors: *

Phone: +39-0116707195, *e*-mail: donatella.boschi@unito.it.

Phone: +39-0116706864, *e*-mail: simona.oliaro@unito.it.

Phone: +39-0116707185, *e*-mail: francesca.spyrakis@unito.it.

Notes. The authors declare no competing financial interest.

Acknowledgements

This research was financially supported by the University of Turin (Ricerca Locale grants BOSD_RILO_20_01, LOLM_RILO_21_01, PIPA_RILO_20_01 and PIPA_RILO_21_01), Fondazione Cassa di Risparmio di Torino (Grant BOSD_CRT_17_2) and TUBITAK (The Scientific and Technological Research Council of Turkey-2219 program). The authors thank Dr Dale James Matthew for proofreading the manuscript.

Appendix A. Supplementary data

Supplementary data related to this article can be found at XXXX.

References

[1] T.M. Penning, AKR1C3 (type 5 17β-hydroxysteroid dehydrogenase/prostaglandin F synthase): Roles in malignancy and endocrine disorders, Molecular and Cellular Endocrinology, 489 (2019) 82-91.
[2] Y. Liu, S. He, Y. Chen, Y. Liu, F. Feng, W. Liu, Q. Guo, L. Zhao, H. Sun, Overview of AKR1C3: Inhibitor Achievements and Disease Insights, J Med Chem, 63 (2020) 11305-11329.
[3] T.M. Penning, S. Jonnalagadda, P.C. Trippier, T.L. Rižner, Aldo-keto reductases and cancer drug resistance, Pharmacological Reviews, 73 (2021) 1150-1171.
[4] S.Q. Sun, X. Gu, X.S. Gao, Y. Li, H. Yu, W. Xiong, H. Yu, W. Wang, Y. Li, Y. Teng, D. Zhou, Overexpression of AKR1C3 significantly enhances human prostate cancer cells resistance to radiation, Oncotarget, 7 (2016) 48050-48058.
[5] A. Altavilla, C. Casadei, C. Lolli, C. Menna, G. Ravaglia, G. Gurioli, A. Farolfi, N. Brighi, V. Conteduca, S.L. Burgio, G. Schepisi, L. Rossi, S. Gargiulo, I. Lisotti, U. De Giorgi, Enzalutamide for the treatment of nonmetastatic castration-resistant prostate cancer, Expert Opin Pharmacother, 21 (2020) 2091-2099.
[6] M.S. Litwin, H.J. Tan, The Diagnosis and Treatment of Prostate Cancer: A Review, Jama, 317 (2017) 2532-2542.
[7] C. Liu, W. Lou, Y. Zhu, J.C. Yang, N. Nadiminty, N.W. Gaikwad, C.P. Evans, A.C. Gao, Intracrine androgens and AKR1C3 activation confer resistance to Enzalutamide in Prostate Cancer, Cancer Res., 75 (2015) 1413-1422.
[8] C. Liu, C.M. Armstrong, W. Lou, A. Lombard, C.P. Evans, A.C. Gao, Inhibition of AKR1C3 activation overcomes resistance to Abiraterone in advanced Prostate Cancer, Mol. Cancer Ther., 16 (2017) 35-44.
[9] K. Verma, N. Gupta, T. Zang, P. Wangtrakluldee, S.K. Srivastava, T.M. Penning, P.C. Trippier, AKR1C3 inhibitor KV-37 exhibits antineoplastic effects and potentiates enzalutamide in combination therapy in prostate adenocarcinoma cells, Mol. Cancer Ther., 17 (2018) 1833-1845.
[10] K. Verma, T. Zang, T.M. Penning, P.C. Trippier, Potent and Highly Selective Aldo-Keto Reductase 1C3 (AKR1C3) Inhibitors Act as Chemotherapeutic Potentiators in Acute Myeloid Leukemia and T-Cell Acute Lymphoblastic Leukemia, J. Med. Chem., 62 (2019) 3590-3616.
[11] J. Hofman, B. Malcekova, A. Skarka, E. Novotna, V. Wsol, Anthracycline resistance mediated by reductive metabolism in cancer cells: the role of aldo-keto reductase 1C3, Toxicol Appl Pharmacol, 278 (2014) 238-248.
[12] X. Li, X. Hong, X. Gao, X. Gu, W. Xiong, J. Zhao, H. Yu, M. Cui, M. Xie, Y. Bai, S. Sun, Methyl jasmonate enhances the radiation sensitivity of esophageal carcinoma cells by inhibiting the 11-ketoprostaglandin reductase activity of AKR1C3, Cancer Manag Res, 10 (2018) 3149-3158.
[13] C. Zhou, Z. Wang, J. Li, X. Wu, N. Fan, D. Li, F. Liu, P.S. Plum, S. Hoppe, A.M. Hillmer, A. Quaas, F. Gebauer, S.-H. Chon, C.J. Bruns, Y. Zhao, Aldo-Keto Reductase 1C3 Mediates Chemotherapy Resistance in Esophageal Adenocarcinoma via ROS Detoxification, Cancers, 13 (2021) 2403.
[14] L. Xie, J. Yu, W. Guo, L. Wei, Y. Liu, X. Wang, X. Song, Aldo-keto reductase 1C3 may be a new radioresistance marker in non-small-cell lung cancer, Cancer Gene Therapy, 20 (2013) 260-266.
[15] Y. Loriot, K. Fizazi, R.J. Jones, J. Van den Brande, R.L. Molife, A. Omlin, N.D. James, E. Baskin-Bey, M. Heeringa, B. Baron, G.M. Holtkamp, T. Ouatas, J.S. De Bono, Safety, tolerability and anti-tumor activity of the androgen biosynthesis inhibitor ASP9521 in patients with metastatic castration-resistant prostate cancer: multi-centre phase I/II study, Invest. New Drugs, 32 (2014) 995-1004.
[16] A.R.N. Santos, H.M. Sheldrake, A.I.M. Ibrahim, C.C. Danta, D. Bonanni, M. Daga, S. Oliaro-Bosso, D. Boschi, M.L. Lolli, K. Pors, Exploration of [2 + 2 + 2] cyclotrimerisation methodology to prepare tetrahydroisoquinoline-based compounds with potential aldo-keto reductase 1C3 target affinity, Medchemcomm, 10 (2019) 1476-1480.
[17] Y. Zhao, X. Zheng, H. Zhang, J. Zhai, L. Zhang, C. Li, K. Zeng, Y. Chen, Q. Li, X. Hu, In vitro inhibition of AKR1Cs by sulphonylureas and the structural basis, Chem.-Biol. Interact., 240 (2015) 310-315.
[18] A. Adeniji, M.J. Uddin, T. Zang, D. Tamae, P. Wangtrakuldee, L.J. Marnett, T.M. Penning, Discovery of (R)-2-(6-Methoxynaphthalen-2-yl)butanoic Acid as a Potent and Selective Aldo-keto Reductase 1C3 Inhibitor, J. Med. Chem., 59 (2016) 7431-7444.
[19] A.J. Liedtke, A.O. Adeniji, M. Chen, M.C. Byrns, Y. Jin, D.W. Christianson, L.J. Marnett, T.M. Penning, Development of Potent and Selective Indomethacin Analogues for the Inhibition of AKR1C3 (Type 5 17β-Hydroxysteroid Dehydrogenase/Prostaglandin F Synthase) in Castrate-Resistant Prostate Cancer, J. Med. Chem., 56 (2013) 2429-2446.

[20] C.M.M. Hendriks, T.M. Penning, T. Zang, D. Wiemuth, S. Gründer, I.A. Sanhueza, F. Schoenebeck, C. Bolm, Pentafluorosulfanyl-containing flufenamic acid analogs: Syntheses, properties and biological activities, Bioorganic & Medicinal Chemistry Letters, 25 (2015) 4437-4440.
[21] M. Sinreih, I. Sosic, N. Beranic, S. Turk, A.O. Adeniji, T.M. Penning, T.L. Rizner, S. Gobec, N-Benzoyl anthranilic acid derivatives as selective inhibitors of aldo-keto reductase AKR1C3, Bioorg Med Chem Lett, 22 (2012) 5948-5951.
[22] M. Chen, A.O. Adeniji, B.M. Twenter, J.D. Winkler, D.W. Christianson, T.M. Penning, Crystal structures of AKR1C3 containing an N-(aryl)amino-benzoate inhibitor and a bifunctional AKR1C3 inhibitor and androgen receptor antagonist. Therapeutic leads for castrate resistant prostate cancer, Bioorg. Med. Chem. Lett., 22 (2012) 3492-3497.
[23] J.S. Choi, M.J. Jin, H.K. Han, Role of monocarboxylic acid transporters in the cellular uptake of NSAIDs, J Pharm Pharmacol, 57 (2005) 1185-1189.
[24] A.C. Pippione, D. Boschi, K. Pors, S. Oliaro-Bosso, M.L. Lolli, Androgen-AR axis in primary and metastatic prostate cancer: chasing steroidogenic enzymes for therapeutic intervention, J Cancer Metastasis Treat, 3 (2017) 328-361.
[25] A.C. Pippione, A. Giraudo, D. Bonanni, I.M. Carnovale, E. Marini, C. Cena, A. Costale, D. Zonari, K. Pors, M. Sadiq, D. Boschi, S. Oliaro-Bosso, M.L. Lolli, Hydroxytriazole derivatives as potent and selective aldo-keto reductase 1C3 (AKR1C3) inhibitors discovered by bioisosteric scaffold hopping approach, Eur. J. Med. Chem., 139 (2017) 936-946.
[26] M.L. Lolli, I.M. Carnovale, A.C. Pippione, W.Y. Wahlgren, D. Bonanni, E. Marini, D. Zonari, M. Gallicchio, V. Boscaro, P. Goyal, R. Friemann, B. Rolando, R. Bagnati, S. Adinolfi, S. Oliaro-Bosso, D. Boschi, Bioisosteres of Indomethacin as Inhibitors of Aldo-Keto Reductase 1C3, ACS Medicinal Chemistry Letters, 10 (2019) 437-443.
[27] A. Kikuchi, T. Furutani, H. Azami, K. Watanabe, T. Niimi, Y. Kamiyama, S. Kuromitsu, E. Baskin-Bey, M. Heeringa, T. Ouatas, K. Enjo, In vitro and in vivo characterisation of ASP9521: a novel, selective, orally bioavailable inhibitor of 17β-hydroxysteroid dehydrogenase type 5 (17βHSD5; AKR1C3), Invest. New Drugs, 32 (2014) 860-870.
[28] K. Verma, T. Zang, N. Gupta, T.M. Penning, P.C. Trippier, Selective AKR1C3 Inhibitors Potentiate Chemotherapeutic Activity in Multiple Acute Myeloid Leukemia (AML) Cell Lines, ACS Medicinal Chemistry Letters, 7 (2016) 774-779.
[29] J.U. Flanagan, G.J. Atwell, D.M. Heinrich, D.G. Brooke, S. Silva, L.J. Rigoreau, E. Trivier, A.P. Turnbull, T. Raynham, S.M. Jamieson, W.A. Denny, Morpholylureas are a new class of potent and selective inhibitors of the type 5 17-beta-hydroxysteroid dehydrogenase (AKR1C3), Bioorg. Med. Chem., 22 (2014) 967-977.
[30] D.M. Heinrich, J.U. Flanagan, S.M.F. Jamieson, S. Silva, L.J.M. Rigoreau, E. Trivier, T. Raynham, A.P. Turnbull, W.A. Denny, Synthesis and structure-activity relationships for 1-(4-(piperidin-1-ylsulfonyl)phenyl)pyrrolidin-2-ones as novel non-carboxylate inhibitors of the aldo-keto reductase enzyme AKR1C3, Eur. J. Med. Chem., 62 (2013) 738-744.
[31] A.C. Pippione, I.M. Carnovale, D. Bonanni, M. Sini, P. Goyal, E. Marini, K. Pors, S. Adinolfi, D. Zonari, C. Festuccia, W.Y. Wahlgren, R. Friemann, R. Bagnati, D. Boschi, S. Oliaro-Bosso, M.L. Lolli, Potent and selective aldo-keto reductase 1C3 (AKR1C3) inhibitors based on the benzoisoxazole moiety: application of a bioisosteric scaffold hopping approach to flufenamic acid, European Journal of Medicinal Chemistry, 150 (2018) 930-945.
[32] A.C. Pippione, S. Sainas, D. Boschi, M.L. Lolli, Hydroxyazoles as acid isosteres and their drug design applications—Part 2: Bicyclic systems, in: Advances in Heterocyclic Chemistry, 2021.
[33] S. Sainas, A.C. Pippione, D. Boschi, M.L. Lolli, Hydroxyazoles as acid isosteres and their drug design applications—Part 1: Monocyclic systems, in: Advances in Heterocyclic Chemistry, 2021.
[34] Y. Amano, T. Yamaguchi, T. Niimi, H. Sakashita, Structures of complexes of type 5 17β-hydroxysteroid dehydrogenase with structurally diverse inhibitors: insights into the conformational changes upon inhibitor binding, Acta Crystallogr D Biol Crystallogr, 71 (2015) 918-927.
[35] S. Sainas, P. Temperini, J.C. Farnsworth, F. Yi, S. Møllerud, A.A. Jensen, B. Nielsen, A. Passoni, J.S. Kastrup, K.B. Hansen, D. Boschi, D.S. Pickering, R.P. Clausen, M.L. Lolli, Use of the 4-Hydroxytriazole Moiety as a Bioisosteric Tool in the Development of Ionotropic Glutamate Receptor Ligands, Journal of Medicinal Chemistry, 62 (2019) 4467-4482.

[36] S. Sainas, A.C. Pippione, A. Giraudo, K. Martina, F. Bosca, B. Rolando, A. Barge, A. Ducime, A. Federico, S.J. Grossert, R.L. White, D. Boschi, M.L. Lolli, Regioselective N-Alkylation of Ethyl 4-Benzyloxy-1,2,3-triazolecarboxylate: A Useful Tool for the Synthesis of Carboxylic Acid Bioisosteres, Journal of Heterocyclic Chemistry, 56 (2019) 501-519.
[37] S. Sainas, A.C. Pippione, M. Giorgis, E. Lupino, P. Goyal, C. Ramondetti, B. Buccinnà, M. Piccinini, R.C. Braga, C.H. Andrade, M. Andersson, A.C. Moritzer, R. Friemann, S. Mensa, S. Al-Kadaraghi, D. Boschi, M.L. Lolli, Design, synthesis, biological evaluation and X-ray structural studies of potent human dihydroorotate dehydrogenase inhibitors based on hydroxylated azole scaffolds, European Journal of Medicinal Chemistry, 129 (2017) 287-302.
[38] K.J. Okolotowicz, P. Bushway, M. Lanier, C. Gilley, M. Mercola, J.R. Cashman, 1,5-Disubstituted benzimidazoles that direct cardiomyocyte differentiation from mouse embryonic stem cells, Bioorg. Med. Chem., 23 (2015) 5282-5292.
[39] S. Sainas, M. Giorgis, P. Circosta, V. Gaidano, D. Bonanni, A.C. Pippione, R. Bagnati, A. Passoni, Y. Qiu, C.F. Cojocaru, B. Canepa, A. Bona, B. Rolando, M. Mishina, C. Ramondetti, B. Buccinnà, M. Piccinini, M. Houshmand, A. Cignetti, E. Giraudo, S. Al-Karadaghi, D. Boschi, G. Saglio, M.L. Lolli, Targeting Acute Myelogenous Leukemia Using Potent Human Dihydroorotate Dehydrogenase Inhibitors Based on the 2-Hydroxypyrazolo[1,5-a]pyridine Scaffold: SAR of the Biphenyl Moiety, Journal of Medicinal Chemistry, 64 (2021) 5404-5428.
[40] K.C. Nicolaou, C.R. Hale, C. Nilewski, H.A. Ioannidou, A. ElMarrouni, L.G. Nilewski, K. Beabout, T.T. Wang, Y. Shamoo, Total synthesis of viridicatumtoxin B and analogues thereof: strategy evolution, structural revision, and biological evaluation, J Am Chem Soc, 136 (2014) 12137-12160.
[41] T.M. Penning, Androgen biosynthesis in castration-resistant prostate cancer, Endocrine-Related Cancer, 21 (2014) T67-T78.
[42] C.W. Murray, D.A. Erlanson, A.L. Hopkins, G.M. Keserü, P.D. Leeson, D.C. Rees, C.H. Reynolds, N.J. Richmond, Validity of Ligand Efficiency Metrics, ACS Medicinal Chemistry Letters, 5 (2014) 616-618.
[43] Y.D. Yin, M. Fu, D.G. Brooke, D.M. Heinrich, W.A. Denny, S.M. Jamieson, The Activity of SN33638, an Inhibitor of AKR1C3, on Testosterone and 17beta-Estradiol Production and Function in Castration-Resistant Prostate Cancer and ER-Positive Breast Cancer, Front. Oncol., 4 (2014) 159.
[44] W. Zhou, P. Limonta, AKR1C3 Inhibition therapy in Castration-Resistant Prostate Cancer and Breast Cancer: lessons from responses to SN33638, Front. Oncol., 4 (2014) 162.
[45] N.M. O'Boyle, M. Banck, C.A. James, C. Morley, T. Vandermeersch, G.R. Hutchison, Open Babel: An open chemical toolbox, Journal of Cheminformatics, 3 (2011) 33.
[46] F. Milletti, L. Storchi, G. Sforna, S. Cross, G. Cruciani, Tautomer Enumeration and Stability Prediction for Virtual Screening on Large Chemical Databases, Journal of Chemical Information and Modeling, 49 (2009) 68-75.
[47] A.C. Pippione, F. Dosio, A. Ducime, A. Federico, K. Martina, S. Sainas, B. Frolund, M. Gooyit, K.D. Janda, D. Boschi, M.L. Lolli, Substituted 4-hydroxy-1,2,3-triazoles: synthesis, characterization and first drug design applications through bioisosteric modulation and scaffold hopping approaches, Medchemcomm, 6 (2015) 1285-1292.
[48] G. Jones, P. Willett, R.C. Glen, A.R. Leach, R. Taylor, Development and validation of a genetic algorithm for flexible docking11Edited by F. E. Cohen, Journal of Molecular Biology, 267 (1997) 727-748.
[49] D.A. Case, V. Babin, J. Berryman, R.M. Betz, Q. Cai, D.S. Cerutti, T. Cheatham, T. Darden, R. Duke, H. Gohlke, A. Götz, S. Gusarov, N. Homeyer, P. Janowski, J. Kaus, I. Kolossváry, A. Kovalenko, T.-S. Lee, P.A. Kollman, AMBER 14, University of California, San Francisco, 2014.
[50] B. Hess, C. Kutzner, D. van der Spoel, E. Lindahl, GROMACS 4: Algorithms for Highly Efficient, Load-Balanced, and Scalable Molecular Simulation, Journal of Chemical Theory and Computation, 4 (2008) 435-447.
[51] S. Decherchi, G. Bottegoni, A. Spitaleri, W. Rocchia, A. Cavalli, BiKi Life Sciences: A New Suite for Molecular Dynamics and Related Methods in Drug Discovery, Journal of Chemical Information and Modeling, 58 (2018) 219-224.
[52] F. Spyrakis, P. Benedetti, S. Decherchi, W. Rocchia, A. Cavalli, S. Alcaro, F. Ortuso, M. Baroni, G. Cruciani, A Pipeline To Enhance Ligand Virtual Screening: Integrating Molecular Dynamics and Fingerprints for Ligand and Proteins, Journal of Chemical Information and Modeling, 55 (2015) 2256-2274.

[53] S. Sciabola, P. Benedetti, G. D'Arrigo, R. Torella, M. Baroni, G. Cruciani, F. Spyrakis, Discovering New Casein Kinase 1d Inhibitors with an Innovative Molecular Dynamics Enabled Virtual Screening Workflow, ACS Medicinal Chemistry Letters, 10 (2019) 487-492.
[54] A.C. Pippione, A. Federico, A. Ducime, S. Sainas, D. Boschi, A. Barge, E. Lupino, M. Piccinini, M. Kubbutat, J.M. Contreras, C. Morice, S. Al-Karadaghi, M.L. Lolli, 4-Hydroxy-: N -[3,5-bis(trifluoromethyl)phenyl]-1,2,5-thiadiazole-3-carboxamide: A novel inhibitor of the canonical NF-κB cascade, MedChemComm, 8 (2017) 1850-1855.
[55] A.C. Pippione, S. Sainas, P. Goyal, I. Fritzson, G.C. Cassiano, A. Giraudo, M. Giorgis, T.A. Tavella, R. Bagnati, B. Rolando, R. Caing-Carlsson, F.T.M. Costa, C.H. Andrade, S. Al-Karadaghi, D. Boschi, R. Friemann, M.L. Lolli, Hydroxyazole scaffold-based Plasmodium falciparum dihydroorotate dehydrogenase inhibitors: Synthesis, biological evaluation and X-ray structural studies, European Journal of Medicinal Chemistry, 163 (2019) 266-280.
[56] S. Sainas, F. Dosio, D. Boschi, M.L. Lolli, Targeting Human Onchocerciasis: Recent Advances Beyond Ivermectin, in: Annual Reports in Medicinal Chemistry, 2018, pp. 1-38.
[57] E. Rubin, A.C. Pippione, M. Boyko, G. Einaudi, S. Sainas, M. Collino, C. Cifani, M.L. Lolli, N. Abu-Freha, J. Kaplanski, D. Boschi, A.N. Azab, A New NF-kappa B Inhibitor, MEDS-23, Reduces the Severity of Adverse Post-Ischemic Stroke Outcomes in Rats, Brain Sciences, 12 (2022) 35.